# *Controlling cis/trans isomerism of monounsaturated fatty acids via a recombinant cytochrome c-type cis/trans fatty acid isomerase*

# Controlling *cis*/*trans* isomerism of monounsaturated fatty acids via a recombinant cytochrome *c*-type *cis*/*trans* fatty acid isomerase

Jun-Young Park[a,1], Yun-Seo Jung[b,1], Dimitris Charalampopoulos[c], Kyung-Min Park[b,*], Pahn-Shick Chang[a,d,e,f,*]

[a] *Department of Agricultural Biotechnology, Seoul National University, Seoul 08826, Republic of Korea*

[b] *Department of Food Science and Biotechnology, Wonkwang University, Iksan 54538, Republic of Korea*

[c] *Department of Food and Nutritional Sciences, University of Reading, Reading RG6 6AP, United Kingdom*

[d] *Research Institute of Agriculture and Life Sciences, Seoul National University, Seoul 08826, Republic of Korea*

[e] *Center for Food and Bioconvergence, Seoul National University, Seoul 08826, Republic of Korea*

[f] *Center for Agricultural Microorganism and Enzyme, Seoul National University, Seoul 08826, Republic of Korea*

[1] Equal contribution as first authors.

* Authors to whom correspondence should be addressed: K. M. Park [telephone: +82 63 850 6681; e-mail: kmpark79@wku.ac.kr] or P. S. Chang [telephone: +82 2 880 4852; e-mail: pschang@snu.ac.kr].

## Abstract

Cytochrome *c*-type *cis*/*trans* fatty acid isomerase (CTI) has been proposed to control *cis*/*trans* isomerism of unsaturated fats in lipid-related food products. A gene encoding wildtype CTI from *Pseudomonas putida* KT2440 was introduced into the pET26b/pEC86 co-expression system, and the heme C cofactor was covalently bound into the expressed CTI protein through *in vivo* cytochrome *c* maturation. The recombinant CTI, purified from *Escherichia coli* BL21(DE3), catalyzed the *cis*/*trans* isomerization of three edible monounsaturated fatty acids. It exhibited strong substrate selectivity for palmitoleic acid ($C_{16:1}$, *cis*-$\Delta^9$), reaching an 80.93±1.78% conversion at reaction equilibrium. Notably, its promiscuity for other fatty acids (oleic acid: 29.21±5.01% and *cis*-vaccenic acid: 51.21±0.05%) was observed. Under the optimum reaction conditions (pH 7.5 and 15℃), the kinetic parameters ($V_{max}$, $K_m$, and $k_{cat}$) of CTI were derived as 0.035 mM·min$^{-1}$, 0.267 mM, and 0.141 sec$^{-1}$, respectively, and the final catalytic efficiency ($k_{cat}/K_m$) was calculated as 5.26 × 10$^2$ M$^{-1}$·sec$^{-1}$. Furthermore, structural properties of CTI were analyzed using deep learning-based protein structure prediction, suggesting the potential for specificity variability by altering loop dynamics and helix interactions surrounding the heme-binding motif. The following results would provide theoretical and practical information for CTI enzymes as novel promising industrial catalysts to control *cis*/*trans* isomerism of lipids in food products.



***Keywords***: *cis*/*trans* fatty acid isomerase; *cis*/*trans* isomerization; *Pseudomonas putida* KT2440; monounsaturated fatty acid; cytochrome *c*; pET26b/pEC86 co-expression system.

## 1. Introduction

In the past three decades, the consumption of industrial *trans*-fatty acids (*i.e.*, unsaturated fatty acids that contain non-conjugated carbon-carbon double bonds in *trans* configuration) has been proposed to be responsible for a higher incidence of coronary heart disease (CVD) (Kodali, 2014). Compared with *cis*-fatty acids, they have a straight aliphatic hydrocarbon chain similar to saturated fatty acids, known to increase the ratio of low-density to high-density lipoprotein cholesterol levels (LDL:HDL) in human blood (greater than that of saturated fatty acids) (Mozaffarian, Aro, & Willett, 2009). Although natural foods such as ruminant meat, dairy products, and refined oils contain *trans*-fatty acids in small amounts, the majority are industrially produced during the hydrogenation process of vegetable/fish oils for manufacturing partially hydrogenated vegetable oils (PHVOs), margarines, and shortenings (Kuhnt, Baehr, Rohrer, & Jahreis, 2011; Mozaffarian, Katan, Ascherio, Stampfer, & Willett, 2006). These detrimental lipids are found in most processed food products containing unsaturated fats because heating or frying operations can induce their production (Tsuzuki, Matsuoka, & Ushida, 2010). The World Health Organization (WHO) has declared that the elimination of *trans*-fatty acids in food products is the most effective intervention to prevent CVDs and create a healthier food supply (Ghebreyesus & Frieden, 2018). Therefore, food scientists have studied relevant scientific technologies – process improvement for hydrogenation (Iida, Takahashi, Yanagisawa, Hashimoto, & Igarashi, 2021), natural hardstock blending (Yamoneka, Malumba, Lognay, Blecker, & Danthine, 2019), trait-enhanced oils (Wilkes & Bringe, 2015), functional additives (Guo et al., 2015), chemical and enzymatic interesterification (Kim & Akoh, 2015), and other techniques (Brundiek, Evitt, Kourist, & Bornscheuer, 2012) – to reduce, remove, or replace *trans*-fatty acids in food products. Despite this, no technology has been developed that allows direct control of *cis*/*trans* isomerization during downstream processing of unsaturated fats.

More recently, it has been proposed that enzymatic *cis*/*trans* isomerization of fatty acids can be an innovative technology to manufacture ideal *trans*-free food products under mild conditions. In a bid to find novel isomerases, our research group has developed an improved method for rapid evaluation of

enzymatic *cis*/*trans* isomerization of monounsaturated fatty acids in a reversed micelle enzyme reaction system (Park, Choi, Park, & Chang, 2023). In this previous study, an enzyme, *cis*/*trans* fatty acid isomerase (CTI) from *Pseudomonas putida*, was initiatively suggested as a promising enzyme resource to be repurposed for catalyzing the *cis*/*trans* isomerization of unsaturated fatty acids. A few *Pseudomonas* strains have evolved a unique strategy based on the *cis*/*trans* isomerization of membrane phospholipids to resist external exposure to hazardous substances (Diefenbach & Keweloh, 1994; Heipieper, Diefenbach, & Keweloh, 1992). Several microbiological studies revealed that CTI, which is a constitutively expressed enzyme, rigidifies cytoplasmic membranes for rapid adaptation to external waves via immediate conversion of the *cis*-fatty acid moiety of membrane phospholipids into their *trans* configurations (Holtwick, Meinhardt, & Keweloh, 1997; Mauger, Ferreri, Chatgilialoglu, & Seemann, 2021). This CTI enzyme is a cytochrome *c*-type hemoprotein with a heme-binding motif (CXXCH) (Holtwick, Keweloh, & Meinhardt, 1999) and functions without a transient saturation of the carbon-carbon double bond during the reaction (von Wallbrunn, Richnow, Neumann, Meinhardt, & Heipieper, 2003), indicating the direct catalysis of isomerization. These findings partially support efforts to introduce the CTI gene into industrial bacterial strains to enhance tolerance and robustness during bioconversion processes (Ahn, Lee, Bang, & Lee, 2018; Tan, Yoon, Nielsen, Shanks, & Jarboe, 2016).

On the other hand, there was no report to facilitate CTI enzymes for the direct *cis*/*trans* isomerization of unsaturated fats in lipid-based food products, although microbial hemoproteins have been investigated as major industrial catalysts that enable manufacturers to selectively produce desired compounds. Only a few wildtype CTIs were isolated and characterized (Okuyama, Ueno, Enari, Morita, & Kusano, 1997; Pedrotta & Witholt, 1999), whereas it has been difficult to mass-produce CTI recombinant proteins via biotechnological methodologies. It was reported that histidine-tagged CTI recombinant proteins from *P. putida* P8 were expressed in a heterologous *Escherichia coli*-pQE60 expression system; however, data on their catalytic activities are unavailable (Holtwick et al., 1999). Since cytochrome *c*-type hemoproteins typically undergo cytochrome *c* maturation during membrane translocation to the

periplasm (a heme C cofactor is covalently bound to the apoprotein during this process) (Thöny-Meyer, 1997), it is highly challenging to forcibly induce expression of CTI to be in a mature form in heterologous strains without relevant functions. This led us to consider that a more advanced expression system for the production of CTI in its active form is firstly needed to evaluate its *in vitro* catalytic properties and further practical applicability as a potent controller for the *cis*/*trans* isomerization of unsaturated lipids. Moreover, no protein structure of CTI has been elucidated via either experimental methods or computational predictions. It is essential to investigate the protein structure and its relationship to the catalytic mechanism to further modify the enzyme tailored to the desired specifications.

In the present study, we have introduced a wildtype CTI gene from *P. putida* KT2440 into a heterologous *E. coli* BL21(DE3) based on the pET26b/pEC86 co-expression system to mass-produce CTI recombinant proteins in their active forms and consequently control the *cis*/*trans* isomerization of unsaturated fats directly. Catalytic properties of the purified CTI recombinant proteins against three different edible *cis*-monounsaturated fatty acids, which can be found in various food sources and products, were evaluated using the reversed micelle reaction system. In addition, the structural properties of CTI were investigated using the latest computational protein structure prediction methodologies to in-depth understand its mode of action, substrate specificity/selectivity, and potential for further adaptation. The following results would provide theoretical and practical information for introducing CTI enzymes as novel promising industrial catalysts to control *cis*/*trans* isomerism of lipids in food products.

## 2. Materials & methods

### *2.1. Materials*

Oleic acid (≥99.0%), elaidic acid (≥98.0%), and kanamycin sulfate (USP standard) were purchased from Thermo Fisher Scientific Co. (Waltham, MA, USA). *Cis*-vaccenic acid (≥97.0%), *trans*-vaccenic acid (≥99.0%), *cis*-11-vaccenic methyl ester (≥95.0%), *trans*-11-vaccenic methyl ester (≥95.0%), methyl oleate (≥98.5%), methyl elaidate (≥99.0%), and dioctyl sulfosuccinate sodium salt (AOT, ≥97.0%)

were purchased from Sigma-Aldrich Co. (St. Louis, MO, USA). Palmitoleic acid (≥98.0%), methyl palmitoleate (≥95.0%), isopropyl β-D-1-thiogalactopyranoside (IPTG, ≥98.0%), and 5-aminolevulinic acid hydrochloride (ALA, ≥98.0%) were purchased from Tokyo Chemical Industry Co. (Tokyo, Japan). Palmitelaidic acid (≥99.0%), methyl palmitelaidate (≥98.0%), and chloramphenicol (≥98.0%) were purchased from Santa Cruz Biotechnology Co. (Santa Cruz, CA, USA). Restriction enzymes (Nco1, Nde1, and Xho1) were purchased from Takara Bio Co. (Shiga, Japan). High performance liquid chromatography-grade *n*-hexane (≥95.0%), ethanol (≥99.0%), and other chemicals (extra pure grade) were purchased from Daejung Chemicals & Metals Co. (Siheung, Republic of Korea).

### *2.2. Plasmids, strains, and media*

Plasmid pET26b(+) (Novagen®) was used as a cloning vector, and cloning was performed through in-fusion cloning. Plasmid pEC86 (Culture Collection of Switzerland) was used for cytochrome *c* maturation (Arslan, Schulz, Zufferey, Künzler, & Thöny-Meyer, 1998). *P. putida* KT2440 strain (ATCC® 47054™), as well as its whole genome sequence, was distributed from American Type Culture Collection (Manassas, VA, USA). Heterologous *E. coli* DH5α (Dyne Bio Co., Seongnam, Republic of Korea) and *E. coli* BL21(DE3) (SoluBL21™, Genlantis Co., San Diego, CA, USA) strains were employed for sub-cloning of plasmid and expression of recombinant protein, respectively. All cells were propagated before use according to manufacturer instructions. The recombinant cells transformed with pET26b(+) or pEC86 plasmids were grown in Luria-Bertani (LB) media with 50 μg/mL kanamycin or 20 μg/mL chloramphenicol, respectively. Cells containing both pET26b(+) and pEC86 plasmids were grown in LB medium with 50 μg/mL kanamycin and 20 μg/mL chloramphenicol ($LB_{kan/chlor}$).

### *2.3. Construction of plasmid and dual-transformation*

Genomic DNA (gDNA) of *P. putida* KT2440 strain was extracted with AccuPrep® Genomic DNA Extraction Kit (Bioneer Co., Daejeon, Republic of Korea). The gene encoding CTI (2,301 bp; Uniprot

ID Q88KB4) was amplified from the gDNA by overhang PCR using Pfu polymerase and two 5′ overhang F/R primers (Fig. 1a). The annealing and extension temperatures of overhang PCR were set to 60℃ and 72℃, respectively. The CTI DNA fragments were detected on 1%(w/v) agarose gel, purified using PureLink™ Quick Gel Extraction and PCR Purification Combo Kit (Thermo Fisher Scientific Co.), and in-fusion cloned using AccuRapid™ Cloning Kit (Bioneer Co.) into the linearized pET26b(+) vectors between restriction enzyme sites *Nco1* and *Xho1* in frame with an N-terminal pelB signal peptide (to promote periplasmic localization and maturation; MKYLLPTAAAGLLLLAAQPAMA) and a C-terminal polyhistidine fusion tag ($His_6$; HHHHHH) (Fig. 1b). Based on the codon usage of *E. coli* provided by the Codon Usage Database (https://www.kazusa.or.jp/codon/), the codon adaptation index (CAI) of the recombinant CTI gene was calculated as follows (Sharp & Li, 1987):

$$Codon\ Adaptation\ Index\ (CAI) = (\prod_{i=1}^{L} w_i)^{\frac{1}{L}}$$

where $w_i$ and $L$ are the codon weight for the $i^{th}$ codon in the gene and the total number of codons in the gene, respectively. Codon weight (*i.e.*, the relative adaptiveness of a codon) is the frequency of codon usage of each codon compared to that of the optimal synonymous codon for the same amino acid. The pEC86 plasmid was also co-introduced to ensure cytochrome *c* maturation in aerobic culture conditions (Fig. 1c). The constructed pET26b(+) plasmids possessing the CTI gene were transformed into *E. coli* BL21(DE3) competent cells by heat shock (42℃, 30 sec) before making them competent cells again, and the pEC86 plasmids were subsequently transformed (Fig. 1d). Chemically competent cells were prepared using calcium chloride ($CaCl_2$) as previously described (Green & Rogers, 2013). *E. coli* BL21(DE3) transformants were selected by antibiotic screening and restriction enzyme treatment, and their plasmids were sequenced by Sanger sequencing (serviced by Bioneer Co.).

*2.4. Expression and purification of recombinant proteins*

An overnight sub-culture (7.5 mL, $LB_{kan/chlor}$) of dual-transformed *E. coli* BL21(DE3) cells, which

contain the constructed pET26b(+) plasmid encoding the CTI gene, as well as the pEC86 plasmid, was inoculated in a three-liter Erlenmeyer flask containing $LB_{kan/chlor}$ broth medium (750 mL) without other carbon sources. This main culture was incubated at 37℃ and 200 rpm (no humidity control) until the optical density ($OD_{600}$) reached 0.6–0.7 (mid-log phase, approximately 2–3 h), and then, the flask was placed on ice (below 4℃) for 30 min. To initiate CTI expression, IPTG and ALA were added to final concentrations of 5 μM and 500 μM, respectively, and the culture was incubated at 20℃ and 200 rpm for 20 h. Cell pellets were collected by centrifugation (4,000*g*, 20 min, 4℃) and stored at –80℃ until further use (at least 24 h). The cell pellets were resuspended in 15 mL of 20 mM Tris-HCl buffer (pH 7.5) containing 10 mM imidazole and 200 mM sodium chloride (NaCl) at room temperature, and the cells were totally lysed by sonication (8 min, 2 sec on, 2 sec off, 12 sec pause per 1 min, 30% power; NE-300Z sonicator, LabTech Co., Jeonju, Republic of Korea) on ice. Cell debris with insoluble proteins was removed by centrifugation (13,000*g*, 20 min, 4℃) and supernatant with soluble proteins was obtained as cleared lysate (approximately 20 mL/batch). The cleared lysate was sterile-filtered through a 0.45 μm cellulose acetate filter and resolved using an ÄKTA go™ fast protein liquid chromatography (FPLC) system (Cytiva Co., Marlborough, MA, USA) equipped with a 1 mL Ni-NTA affinity column (HisTrap™ High Performance; Cytiva Co.) and ultraviolet (UV) detector. His-tagged CTI recombinant proteins were eluted by running a linear imidazole gradient (10 to 500 mM) over 15 column volumes (1 mL/min, 0.5 mL fraction). The purity of each fraction was analyzed by SDS-PAGE analysis, and then, pure fractions were collected, dialyzed overnight in 50 mM potassium phosphate buffer (pH 7.5) using a 10 kDa molecular weight cut-off (MWCO) dialysis sack (Thermo Fisher Scientific Co.), and concentrated via a 50 kDa MWCO centrifugal filter (Sigma-Aldrich Co.). Protein concentration was measured by the Bradford assay using bovine serum albumin as the standard protein.

### *2.5. CTI activity assay*

The CTI activity against monounsaturated fatty acids was determined in a reversed micelle reaction

system, as previously described (Park et al., 2023). In detail, 0.09 mL of the purified CTI dissolved in 50 mM potassium phosphate buffer (pH 7.5) was added to 4.41 mL of 113.38 mM AOT/isooctane (10 of *R*-value) before vigorous vortexing for 1 min to produce stable reversed micelles (reaction medium). The reaction medium with a magnetic stirrer was pre-incubated for 10 min at 20℃ and 800 rpm, and the reaction was initiated by adding 0.5 mL of substrate dissolved in isooctane. After the CTI reaction, an aliquot of the reactant (300 μL) was sampled, and then, isooctane was totally removed by evaporation at room temperature using a nitrogen evaporator (MGS-3100; Eyela Co., Bohemia, NY, USA). Fatty acids in the dried reactants were methylated using a Fatty Acid Methylation Kit (Nacalai Tesque Co., Kyoto, Japan) according to manufacturer instructions. The dried samples were sufficiently dissolved with 0.5 mL of methylation reagent A (toluene:methanol=52:48, v/v) and 0.5 mL of methylation reagent C (strong acidic $BF_3$-methanol solution) before incubation for 20 min at 37℃. Generated fatty acid methyl esters (FAMEs) were fractionated with *n*-hexane (1 mL), followed by washing with deionized water (1 mL). The washed samples were filtered through a 0.45 μm PTFE filter and analyzed through a YL6500 gas chromatography (GC) system (Young In Chromass Co., Anyang, Republic of Korea) equipped with a cyanopropyl phase DB-FastFAME capillary column (30 m × 0.25 mm × 0.25 μm; Agilent Technologies Co., Santa Clara, CA, USA) and a flame ionization detector (FID). Helium (≥99.999%) was used as a carrier gas at a flow rate of 1.0 mL/min (constant flow), and other details of GC-FID analysis are summarized in Supplementary Data Table S1. Calibration curves for methyl oleate, methyl elaidate, methyl *cis*-vaccenate, and methyl *trans*-vaccenate were adapted from our previous study (Park et al., 2023). Calibration curves for methyl palmitoleate and palmitelaidate, together with resolution factor, were newly derived in the present study (Supplementary Data Fig. S2). The separation of adjacent peaks was characterized by resolution factor ($R_s$) as follows:

$$Resolution\ factor\ (R_s) = 1.18 \times \left[\frac{t_{R2} - t_{R1}}{W_{h2} + W_{h1}}\right]$$

where $t_R$ is the retention time for each peak, $W_h$ is the full width at half maximum of each peak, and an

indexed number (1 and 2) refers to the former and the latter of adjacent peaks, respectively. The catalytic activity of CTI was assessed by calculating the conversion rate (%) of *cis* configuration to *trans* configuration as follows:

$$Conversion\ rate\ (\%) = \frac{[trans]_t}{[cis]_t + [trans]_t} \times 100$$

where $[cis]_t$ and $[trans]_t$ are the amounts of fatty acid in *cis* and *trans* configuration at specific reaction time *t*, respectively. For the kinetic analysis, the reaction under given conditions was analyzed based on the Michaelis-Menten assumption using SigmaPlot software (ver. 12.5; Systat Software Co., San Jose, CA, USA). The Michaelis-Menten assumption was validated by Hanes-Woolf double-reciprocal plotting as follows:

$$\frac{[S]}{v} = \frac{1}{V_{max}} \times [S] + \frac{K_m}{V_{max}}$$

where [*S*] is the concentration of substrate, *v* is the initial velocity of the reaction, $V_{max}$ is the maximum initial velocity of the reaction, and $K_m$ is the dissociation constant of the enzyme-substrate complex.

### *2.6. Genome-based computational analysis of protein structure*

Both an original CTI gene (Uniprot ID Q88KB4) encoded in the gDNA of *P. putida* KT2440 and a recombinant CTI gene encoded in the constructed pET26b(+) plasmid (Supplementary Data Fig. S3) were used for computational protein structure prediction. Signal peptide type, subregions, and cleavage site were predicted from the genes using SignalP 6.0 software (https://services.healthtech.dtu.dk/services/SignalP-6.0/), which is based on a transformer protein language model trained on a massive dataset of unlabeled amino acid sequences (Teufel et al., 2022). The likelihoods of signal peptide at each amino acid residue were expressed as region probabilities (*P*), and cleavage sites were predicted in the correct signal peptide type. Three-dimensional (3D) model for a target protein was predicted from the gene through deep learning-based RoseTTAFold software (https://robetta.bakerlab.org/), which is a

prediction architecture with a three-track deep neural network to acquire relationships within and between amino acid sequences, distances, and coordinates in the protein structure simultaneously (Baek et al., 2021). Angstrom error estimates of amino acid residues in the predicted model were calculated using a deep learning framework (DeepAccNet) to guide protein structure refinement, and the confidence value (accuracy; 1.0 good, 0.0 bad) of the prediction was derived from the local distance difference test (lDDT) score (Hiranuma, Park, Baek, Anishchenko, Dauparas, & Baker, 2021). The final 3D structure model of protein and ligand was rendered using PyMOL software (https://pymol.org/2/) and UCSF Chimera software (https://www.cgl.ucsf.edu/chimera/) (Pettersen et al., 2004).

## 3. Results & discussion

### *3.1. Molecular cloning of CTI gene in the pET26b/pEC86 co-expression system*

Cytochrome *c*-type CTIs are occasionally discovered in small amounts in Gram-negative bacteria (mainly *Pseudomonas* and *Vibrio* species), and these enzymes are constitutively expressed to ensure their high adaptability in harsh environments (Eberlein, Baumgarten, Starke, & Heipieper, 2018). We selected *P. putida* KT2440 as a source of genes because its catalytic activity in the form of a periplasmic extract was putatively identified against monounsaturated fatty acids in a previous study, and its complete genome sequence was revealed (Nelson et al., 2002; Park et al., 2023). One copy of the gDNA of *P. putida* KT2440 (ATCC® 47054™) strain consists of 6,185,012 base pairs and 5,650 coding sequences, and a putative gene encoding CTI (Uniprot ID Q88KB4) corresponds to 2,708,078–2,710,378 base pairs (2,301 bp/766 amino acids, Supplementary Data Fig. S4a). A BLAST analysis, using this CTI gene from *P. putida* KT2440 as a reference, revealed that the majority of putative CTI genes in *Pseudomonas* strains are highly conserved, with an average sequence identity of 90% (data not shown). Computational prediction of the protein structure based on the nucleotide sequence found two important structural features of the putative CTI protein from *P. putida* KT2440 (Supplementary Data Fig. S4b). One is an N-terminal signal peptide (MVHRILAGAFAKKOSGAVFG, 1–20 amino

acid residues), and the other is an iron-containing heme-binding motif (CVACH, 43–47 amino acid residues) right after 23 amino acid residues from the signal peptide. These results indicate that expressed CTI proteins are localized in the periplasm and undergo post-translational cytochrome *c* maturation during translocation. Indeed, the catalytic activities of all previously reported CTIs from *Pseudomonas* strains were found in their periplasmic fraction (Okuyama et al., 1997; Park et al., 2023; Pedrotta et al., 1999).

Gram-negative bacteria possess a distinct space between the inner cytoplasmic membrane and the outer membrane, known as the periplasm. Most protective enzymes, constitutively expressed in Gram-negative bacteria, are typically located in the periplasm because they are needed to respond to immediate changes in the external environment. These enzymes are initially produced within the cytoplasm in unfolded forms, and signal peptides at their N-terminals are then recognized by the Sec-dependent secretory system for translocation across the cytoplasmic membrane (Owji, Nezafat, Negahdaripour, Hajiebrahimi, & Ghasemi, 2018). Computational prediction of the signal peptide in the wildtype CTI from *P*. *putida* KT2440 revealed the presence of a signal peptide at its N-terminus, which is expected to be recognized by the Sec pathway and cleaved by a signal peptidase I (Sec/SP1-type) (Supplementary Data Fig. S4c). The cleavage site of the signal peptide was predicted to be between the 20$^{th}$ and 21$^{st}$ amino acid residues, and the molecular weight of the wildtype CTI after cytochrome *c* maturation is calculated as approximately 85 kDa. This native signal peptide is known to work similarly in other Gram-negative bacteria, such as *E. coli* (Tan et al., 2016); however, substituting it with a pelB signal peptide (MKYLLPTAAAGLLLLAAQPAMA) can significantly enhance the periplasmic localization of CTI proteins in heterologous *E. coli* BL21(DE3), due to the structural differences in their subregions (n-, h-, and c-region) that are responsible for translocation capacity and efficiency (Owji et al., 2018). Therefore, a pET26b(+) plasmid, encoding a *pelB* signal sequence and a polyhistidine fusion tag upstream and downstream of the multiple cloning site, respectively, was selected as an expression vector for the cloning of the putative CTI gene from *P*. *putida* KT2440 in *E*. *coli* (Fig. 1b).

Furthermore, the wildtype CTI from *P*. *putida* KT2440 is identified as a cytochrome *c*-type protein because of its putative heme-binding motif. Cytochrome *c* is a metalloprotein that contains a covalently bound heme as a prosthetic group, which is capable of undergoing oxidation and reduction (or binding with other compounds) as its iron converts between the ferrous ($Fe^{2+}$) and ferric ($Fe^{3+}$) forms (Thöny-Meyer, 1997). In bacteria, heme attachment to expressed apocytochrome polypeptides by two thioether bonds occurs in the periplasm by a specific membrane protein complex after their translocation across the cytoplasmic membrane (Thöny-Meyer, 1997). This post-translational modification of proteins is called cytochrome *c* maturation, and CTI proteins must covalently bind with a heme cofactor at their heme-binding motifs (CXXCH) to catalyze the *cis*/*trans* isomerization of unsaturated fats. Unfortunately, cytochrome *c* maturation genes (*ccmABCDEFGH*) are endogenously present on the chromosome of *E*. *coli* and function under anaerobic respiratory conditions (Thöny-Meyer, Fischer, Künzler, Ritz, & Hennecke, 1995). To overcome this limitation, a pEC86 plasmid, encoding the relevant genes constitutively expressed from the *tet* promoter (Arslan et al., 1998), was adopted as part of the co-expression system (Fig. 1c). The pEC86 plasmid has been used to complement heterologous expression of recombinant cells harboring cytochrome *c*-type proteins under aerobic respiratory culture conditions to enzymatically synthesize enantiomeric compounds (Kan, Huang, Gumulya, Chen, & Arnold, 2017). Considering these structural features, the wildtype CTI gene from *P*. *putida* KT2440 was in-fusion cloned into *E*. *coli* BL21(DE3) based on the pET26b/pEC86 co-expression system (Fig. 1d).

Under annealing temperature gradient conditions, overhang PCR was performed to amplify a single CTI fragment (2,274 bp) with the desired 5′ overhang from the gDNA of *P*. *putida* KT2440 (Fig. 2a). A clear single DNA band for amplified CTI DNA fragments was detected between 2.0 kb and 3.0 kb under all temperature conditions, and that of 60.0ºC without unspecific DNA bands and smearing was further purified. The purified DNA fragments were in-fusion cloned into linearized pET26b(+) vectors (5,360 bp), in frame with an N-terminal *pelB* signal peptide and a C-terminal polyhistidine fusion tag,

resulting in pET26b(+)-CTI plasmids (7,538 bp) (Fig. 2b). Notably, the pET26b(+) vectors were linearized through two restriction enzymes, *Nco*1 (CCATGG) and *Xho1* (CTCGAG), and after in-fusion cloning, the restriction site of *Nco1* disappeared in the pET26b(+)-CTI plasmids (Supplementary Data Fig. S3). Instead, the restriction enzyme site of *Nde1* (CATATG) at nucleotide position –3 to +2 of the translational start codon (ATG) of the open reading frame was used to confirm the insertion of a CTI gene. Two plasmids, pET26b(+)-CTI and pEC86, were transformed into *E. coli* BL21(DE3) competent cells, and the transformants were screened for antibiotic resistance. Dual-transformants possessing both plasmids were confirmed by gel electrophoresis (Fig. 2c) and sequencing. In addition, each plasmid is recommended to be individually transformed because it was empirically challenging to simultaneously transform both pET26b(+)-CTI and pEC86 plasmids into competent cells.

### *3.2. Heterologous expression of CTI recombinant protein*

Recombinant CTIs with an N-terminal pelB signal peptide and a C-terminal polyhistidine fusion tag (Fig. 3a) were expressed in the pET26b/pEC86 co-expression system under IPTG induction and ALA supplement, and their mature proteins were purified in soluble form by affinity chromatography. First of all, according to computational prediction, the recombinant CTI, which carries a pelB signal peptide, is capable of being recognized by the Sec pathway and translocated into the periplasm of Gram-negative bacteria (Fig. 3b), as intended. The cleavage site of the signal peptide was predicted to be between the 22$^{nd}$ and 23$^{rd}$ amino acid residues, and consequently, the molecular weight of the recombinant CTI after cytochrome *c* maturation is calculated as approximately 86 kDa, which is slightly higher than that of the wildtype CTI, due to the attached polyhistidine fusion tag. However, although the signal peptide of the recombinant CTI was adjusted, and its codon bias (0.75 of CAI value) was low enough to allow heterologous expression in *E. coli* (Supplementary Data Fig. S5), the CTI proteins were obtained in an insoluble form when expressed without dual-transformation of a pEC86 plasmid. Only a few soluble CTI proteins were purified using solubilizing buffers containing 1%(w/v) cationic CHAPS detergents,

and the purified CTI proteins had an incorrect size (below 75 kDa) and exhibited no catalytic activity (Supplementary Data Fig. S6). It was probably due to the lack of cytochrome *c* maturation in CTI.

Cytochrome *c*-type hemoproteins need post-translational maturation in which the heme C cofactor is covalently bound to the heme-binding motif. Correct incorporation of heme molecules into recombinant cytochrome *c*-type apoprotein is essential for the solubility and catalytic activity of its holoprotein in heterologous expression (Arslan et al., 1998; Varnado & Goodwin, 2004). Furthermore, a sufficient supply of heme precursor (ALA) is crucial for the overexpression of recombinant hemoproteins because a shortage of heme to be conjugated with overexpressed hemoproteins leads to the production of immature proteins (Ramzi, Hyeon, & Han, 2015), which can destabilize proteins and cause inclusion bodies or reduced catalytic activity. The pET26b/pEC86 co-expression system with the ALA supplement successfully mass-produced recombinant CTIs in mature form, and consequently, their stability and solubility dramatically increased. His-tagged recombinant CTIs were purified from cleared lysates of the transformant at 227.14–277.80 mM imidazole (28–30 fractions, 0.5 mL/fraction) in Ni-NTA affinity chromatography (Fig. 3c–d). The detected molecular weights of eluted proteins in those pure fractions were between 75 kDa and 100 kDa (Fig. 3e), which corresponds to that of the recombinant CTI (approximately 86 kDa). Several small protein bands (similar to those of incorrect recombinant proteins from the single pET26b(+) expression system) were detected, indicating that unknown destabilized proteins were partially produced during overexpression. Of course, the recombinant CTI proteins were completely purified after chromatographic resolution, as well as dialysis and concentration. These results suggest that the pET26b/pEC86 co-expression system is highly suitable for the heterologous expression of cytochrome *c*-type CTI from *P. putida* KT2440 in *E. coli*.

### *3.3. Catalytic properties of CTI against monounsaturated fatty acids*

The original catalytic activity of CTI in the bacterial periplasm is known for converting *cis*-unsaturated fatty acid moieties of membrane phospholipids into their *trans* configurations (Holtwick et al.,

1999). On the other hand, wildtype CTIs purified from *Pseudomonas* showed catalytic activity on monounsaturated fatty acids, especially palmitoleic acid, under *in vitro* reaction conditions (Okuyama et al., 1997; Pedrotta et al., 1999). Based on these findings, the catalytic activity of the purified recombinant CTI against three edible monounsaturated fatty acids in *cis* configuration – oleic acid ($C_{18:1}$, *cis*-$\Delta^9$), *cis*-vaccenic acid ($C_{18:1}$, *cis*-$\Delta^{11}$), and palmitoleic acid ($C_{16:1}$, *cis*-$\Delta^9$) – was evaluated by conducting the reaction under the reversed micelle reaction system and tracking the formation of *trans*-fatty acids over reaction time until reaching reaction equilibration (Fig. 4a). The GC-FID peaks corresponding to their FAMEs in both *cis* and *trans* configurations were simultaneously observed in the GC-FID chromatograms at the early stage of the reaction (Supplementary Data Fig. S7). The catalytic activity of the wildtype CTI from *P. putida* KT2440, which was detected in the periplasmic extract (Park et al., 2023), was maintained after molecular cloning and heterologous expression in *E. coli*. Notably, the recombinant CTI showed strong substrate selectivity towards palmitoleic acid, similar to the previous results, although it exhibited unique promiscuous substrate specificity for other monounsaturated fatty acids. The final conversion rate (%) of oleic acid, *cis*-vaccenic acid, and palmitoleic acid at reaction equilibration was calculated as 29.21±5.01%, 51.21±0.05%, and 80.93±1.78%, respectively (Fig. 4b). Consequently, the most efficient substrate for the recombinant CTI was palmitoleic acid, which is the major unsaturated fatty acid moiety of membrane phospholipids in *P. putida* KT2440 (Muñoz-Rojas, Bernal, Duque, Godoy, Segura, & Ramos, 2006). These results indicate that CTI catalysis under purified state only favors the formation of *trans* isomers, reminiscent of its original activity in the periplasm (Fischer, Schauer, & Heipieper, 2010), and its protein structure around the heme-binding motif (active site) may be oriented towards its original targets, palmitoleic acid or *cis*-vaccenic acid, over oleic acid (rarely found in bacteria). Nevertheless, the recombinant CTI may have a more relaxed or larger hydrophobic pocket than other wildtype CTIs, considering its promiscuous substrate specificity for unsaturated fatty acids with different alkyl chain lengths or double bond positions. This promiscuity can be exploited for controlling *cis*/*trans* isomerism of unsaturated fats in lipid-related food products.

Moreover, the effects of physicochemical conditions (pH and temperature) on the catalytic activity of the recombinant CTI from *P. putida* KT2440 were investigated to determine its optimum reaction conditions against its major substrate, palmitoleic acid (Fig. 5). First, at the same reaction temperature (20℃), the catalytic activity of the recombinant CTI exhibited a typical bell-shaped curve with a broad peak occurring around pH 5.0–9.0 (Fig. 5a). The relative activity of CTI peaked at pH 7.5 and declined sharply when the pH deviated from that value, resulting in a 70% reduction in activity at either pH 5.0 or pH 9.0. It was highly similar to the behavior of wildtype CTIs from different *Pseudomonas* strains (Okuyama et al., 1997; Pedrotta et al., 1999). These results indicate that CTI is optimized for the conditions of the bacterial periplasm, which maintains a pH value around 7.0–8.0 (Wilks & Slonczewski, 2007), and also this neutral pH range corresponds to the optimal growth condition for *Pseudomonas* bacteria. Compared with this, which is influenced by amino acid composition (mainly side chains), the recombinant CTI exhibited a unique catalytic response depending on the reaction temperature (Fig. 5b). Most bacterial enzymes, including the wildtype CTIs (Okuyama et al., 1997; Pedrotta et al., 1999), have their optimum reaction temperature in the range of 25–45℃, which is ideal for mesophilic bacterial growth. However, the highest catalytic activity of the recombinant CTI from mesophilic *P. putida* KT2440 was observed at 15℃ and retained approximately 90% of its activity at relatively low reaction temperatures (5–10℃). It showed a significant decline above 20°C, being experimentally undetectable beyond 50°C. This peculiar property of the recombinant CTI was likely due to the presence of a C-terminal polyhistidine fusion tag and induced expression in a heterologous strain at low temperature, which could result in a slight discrepancy in protein folding and, consequently, structural instability of the cytochrome *c* domain. Of course, it is necessary to compare it with the wildtype CTI purified from *P. putida* KT2440 or the recombinant CTI protein without any fusion tag or additional amino acids.

Finally, under optimum reaction conditions (pH 7.5 and 15℃), the exploratory kinetic parameters of the recombinant CTI from *P. putida* KT2440 against palmitoleic acid were determined (Fig. 6). The

initial velocity at each palmitoleic acid concentration (0.10–1.20 mM) was derived from a linear regression of the time-course CTI reaction (0–30 min). The CTI reaction was dependent on the substrate concentration and followed a typical Michaelis-Menten enzyme kinetic model (Fig. 6a), as expected in our previous study (Park et al., 2023). The values of $V_{max}$ and $K_m$ were determined as 0.035 mM·min$^{-1}$ and 0.267 mM based on Hanes-Woolf double-reciprocal plotting (Fig. 6b). From these kinetic parameters, the values of turnover number ($k_{cat}$) and catalytic efficiency ($k_{cat}/K_m$) were calculated as 0.141 sec$^{-1}$ and $5.26 \times 10^2$ M$^{-1}$·sec$^{-1}$, respectively. Notably, the recombinant CTI exhibited stronger activity than the periplasmic extract containing the same enzyme, considering the differences in enzyme purity and substrate (palmitoleic acid versus oleic acid). One previous study on CTI purified from *Pseudomonas* sp. strain E-3 determined the kinetic parameters using palmitoleic acid as a substrate (Okuyama et al., 1997). The substrate affinity ($1/K_m$) of this wildtype CTI (8.50 mM$^{-1}$) appears to be relatively higher than our recombinant CTI (3.75 mM$^{-1}$) in magnitude, whereas its unique substrate promiscuity revealed in the present study is considered to be a superior property for controlling *cis*/*trans* isomerism of unsaturated fats in lipid-related food products. Therefore, in future studies, it should be investigated whether the enzyme kinetic properties of the recombinant CTI are actually dissimilar between various kinds of unsaturated fatty acids and acylglycerol species.

### *3.4. Prediction of CTI protein structure and its structural characteristics*

To understand catalytic characteristics and develop biotechnologically engineered CTI enzymes for practical application by rational design or directed evolution, it is imperative to elucidate their protein structures. Unfortunately, there is currently no protein structure information available in the Protein Data Bank for CTIs and their protein homologs. For this reason, in the present study, a genome-based protein 3D structure for the recombinant CTI from *P. putida* KT2440 was proposed by RoseTTAFold structure prediction (Fig. 7). Based on its amino acid sequence, RoseTTAFold predicted various mod-

els for protein 3D structures with atomic precision and calculated the probability density for the distance (Å) between each amino acid residue pair (Baek et al., 2021). We removed an N-terminal pelB signal peptide region (1–22 amino acid residues) up to the putative cleavage site to predict the tertiary protein structure of the recombinant CTI in mature form. After RoseTTAFold prediction, the heme C cofactor with an iron ion as the central atom was computationally aligned in close proximity to the heme-binding motif (active site) of the apoprotein. The estimated confidence value for the best protein structure model was calculated as 0.80, which indicates that the model is of high accuracy. The angstrom error estimates for each amino acid residue of the best model ranged from 0.64 to 10.56 Å, while amino acid residues except the N-terminus (signal peptide-cleaved pro-region) and the C-terminus (polyhistidine fusion tag) were below 4.00 Å (Supplementary Data Fig. S8).

The truncated N-terminal loop region (23–32 amino acid residues after the cleavage site), containing hydrophobic amino acids (hydrophobic:neutral=6:4), was predicted with slight imprecision since predicting the folding state of the pro-region after cleavage and translocation by the Sec-dependent secretory pathway still remains a challenge. In contrast, the cytochrome c domain region (comprising amino acid residues 33–190) consisting of six short α-helices, several extra loops, and a heme-binding motif (CVACH, amino acid residues 46–50), was predicted to be well-folded in state, probably due to its high structural homology with other cytochrome hemoproteins from varied origins. The formation of cytochrome *c*-type hemoproteins involves two thioether bonds between the two vinyl groups of heme and two cysteine thiol groups in the heme-binding motif of the apoprotein (Thöny-Meyer, 1997). Therefore, to ensure proper protein folding into the final tertiary structure, the heme C cofactor must be covalently bound to the two thiol groups of cysteines (Cys46 and Cys49) in the heme-binding motif of the recombinant CTI through post-translational cytochrome *c* maturation. The central iron ion ($Fe^{2+}$) of heme is axially coordinated to the proximal side chain of a histidine ligand (His50), which is also strictly conserved in the heme-binding motif. The other axial coordination site of heme remains to be

coordinated by distal substrate ligands, in the case of CTI, the carbon-carbon double bond in unsaturated fatty acids or phospholipids. Notably, loop dynamics and helix interactions around the heme-binding motif (active site) can determine the substrate binding properties of CTI, and it may be conserved to favor its original substrates, especially palmitoleic acid. Nevertheless, the size of the binding pocket and substrate tunnel in the predicted CTI model (Fig. 7, bottom view) is large to accommodate a wide range of unsaturated fatty acids and acylglycerol species, determining its promiscuous substrate specificity. Moreover, this predicted CTI structure suggests that its substrate specificity and selectivity can be artificially altered and reinforced through directed evolution or rational protein engineering. Of course, the actual shape and molecular dynamics of this space should be further elucidated by experimental determination like X-ray crystallography for a more in-depth investigation of this.

In Gram-negative bacteria, the cytochrome *c* maturation of hemoproteins is tightly linked to the Sec pathway and occurs in concert with membrane translocation of apoprotein (Sec/SP1), membrane translocation of heme (ccmA–D), and shuttling/attachment of heme to the apoprotein (ccmE-G) (Stevens, Mavridou, Hamer, Kritsiligkou, Goddard, & Ferguson, 2011). A heme-binding motif oxidizes to form disulfides that are reduced by ccmG, and the apoprotein and a heme cofactor are coupled by the heme lyase ccmF before ccmH recognizes CXXCH motifs to receive heme from ccmE and covalently attach it to the heme-binding motif (Brausemann, Zhang, Ilcu, & Einsle, 2021). During these comprehensive processes, protein folding of hemoproteins occurs without any known involvement of other chaperones (Thöny-Meyer, 1997), and in other words, the tertiary structure of the cytochrome *c* domain depends on its amino acid sequence. This process demonstrates that the recombinant CTI, when heterologously expressed in *E. coli*, can exhibit substrate specificity similar to that of the wildtype CTI. It also suggests that it is possible to modulate the molecular dynamics of loop and helix structures around the heme-binding motif through genetic mutations of specific amino acid residues. In addition, the CTI from *P. putida* KT2440 has a larger structure than other cytochrome *c* hemoproteins (usually 10–20 kDa). The

roles of other protein domains (191–760 amino acid residues) are still unknown, and homology structure alignments failed to identify similar structures with high identity (above 30%). These three individual domains are structurally similar (Fig. 7, side view), containing one β-sheet and several α-helices, and the cytochrome *c* domain is completely covered with these bulky domains like a sunshade parasol (Fig. 7, top view). Not fully understood, it was theoretically proposed that CTI activity in the periplasm is regulated by enabling the enzyme to access phospholipids in the cytoplasmic membrane (Heipieper et al., 2001). A catalytic cytochrome *c* domain of CTI may be only accessible to the target if cytoplasmic membranes are disintegrated by external stresses that increase membrane fluidity. The bulky domain in the predicted model may hinder the enzyme from fully embedding or penetrating the cytoplasmic membrane, resulting in it being partially intercalated into the lipid bilayer at the appropriate depth for the *cis*/*trans* isomerization of fatty acid moieties. These structural properties of CTI will be invaluable when applied to lipid-related food products containing oil droplets or bulky oils, as the hydrophilic enzyme faces challenges accessing the substrate in such contexts.

## 4. Conclusions

Using food lipid compounds as reactants, such as edible oils and fats, microorganisms are practically limited, and a single enzyme needs to be employed, either in free or immobilized form. More recently, a cytochrome *c*-type CTI from Gram-negative bacteria has been proposed as a promising enzyme to facilitate the direct control of *cis*/*trans* fatty acid isomerization in lipid-related food products without saturation, hydrolysis, and other additional processes. In the present study, a heterologous expression platform for CTI from *P*. *putida* KT2440 was established based on the pET26b/pEC86 co-expression system. The recombinant CTI was successfully expressed in *E*. *coli* BL21(DE3) and purified in highly soluble and active form by Ni-NTA affinity chromatography. Then, its catalytic activity on three different monounsaturated fatty acids was evaluated in a reversed micelle reaction system and revealed

its unique promiscuous substrate specificity. Furthermore, computational prediction of the protein tertiary structure for the recombinant CTI was performed to demonstrate its folding and enzymatic nature, forming the basis for biotechnological manipulation of its synthetic capabilities. These results provide theoretical information for investigating CTI enzymes in biotechnological processes, and hopefully, the *cis*/*trans* isomerization of unsaturated lipids will be added to the extensive processing repertoire of the food and lipid industry. Of course, at present, recombinant CTI with robustness and promiscuity can serve as an enzyme resource for manufacturing both *trans*-fatty acids and *cis*/*trans* isomer mixtures under mild conditions in the various fields because CTI catalysis favors the formation of *trans* isomers.

## CRediT Authorship Contribution Statement

**Jun-Young Park**: Conceptualization, Investigation, Data curation, Writing - Original draft, Writing - Review & Editing, Visualization. **Yun-Seo Jung**: Investigation, Validation, Formal analysis, Writing - Review & Editing. **Dimitris Charalampopoulos**: Writing - Review & Editing. **Kyung-Min Park**: Writing - Review & Editing, Project administration, Funding acquisition. **Pahn-Shick Chang**: Conceptualization, Writing - Review & Editing, Supervision, Project administration.

## Declaration of Competing Interest

The authors declare that they have no known competing financial interests or personal relationships that could have appeared to influence the work reported in this paper.

## Acknowledgments

This work was carried out with the supports of the National Research Foundation of Korea (NRF) grant funded by the Korea government (MSIT) (No. 2020R1C1C1009678) and "Cooperative Research Program for Agriculture Science & Technology Development (Project No. PJ01488802)" provided by Rural Development Administration, Republic of Korea.

## Data Availability

Data will be made available on request.

## References


Ahn, J. H., Lee, J. A., Bang, J., & Lee, S. Y. (2018). Membrane engineering via *trans*-unsaturated fatty acids production improves succinic acid production in *Mannheimia succiniciproducens*. *Journal of Industrial Microbiology and Biotechnology, 45*(7), 555-566. https://doi.org/10.1007/s10295-018-2016-6

Arslan, E., Schulz, H., Zufferey, R., Künzler, P., & Thöny-Meyer, L. (1998). Overproduction of the *Bradyrhizobium japonicum c*-type cytochrome subunits of the $cbb_3$ oxidase in *Escherichia coli*. *Biochemical and Biophysical Research Communications, 251*(3), 744-747. https://doi.org/10.1006/bbrc.1998.9549

Baek, M., DiMaio, F., Anishchenko, I., Dauparas, J., Ovchinnikov, S., Lee, G. R., . . . Baker, D. (2021). Accurate prediction of protein structures and interactions using a three-track neural network. *Science, 373*(6557), 871-876. https://doi.org/10.1126/science.abj8754

Brausemann, A., Zhang, L., Ilcu, L., & Einsle, O. (2021). Architecture of the membrane-bound cytochrome *c* heme lyase CcmF. *Nature Chemical Biology, 17*(7), 800-805. https://doi.org/10.1038/s41589-021-00793-8

Brundiek, H. B., Evitt, A. S., Kourist, R., & Bornscheuer, U. T. (2012). Creation of a lipase highly selective for *trans* fatty acids by protein engineering. *Angewandte Chemie International Edition, 51*(2), 412-414. https://doi.org/10.1002/anie.201106126

Diefenbach, R., & Keweloh, H. (1994). Synthesis of *trans* unsaturated fatty acids in *Pseudomonas*

*putida* P8 by direct isomerization of the double bond of lipids. *Archives of Microbiology, 162*(1), 120-125. https://doi.org/10.1007/BF00264384

Eberlein, C., Baumgarten, T., Starke, S., & Heipieper, H. J. (2018). Immediate response mechanisms of Gram-negative solvent-tolerant bacteria to cope with environmental stress: *Cis-trans* isomerization of unsaturated fatty acids and outer membrane vesicle secretion. *Applied Microbiology and Biotechnology, 102*(6), 2583-2593. https://doi.org/10.1007/s00253-018-8832-9

Fischer, J., Schauer, F., & Heipieper, H. J. (2010). The *trans*/*cis* ratio of unsaturated fatty acids is not applicable as biomarker for environmental stress in case of long-term contaminated habitats. *Applied Microbiology and Biotechnology, 87*(1), 365-371. https://doi.org/10.1007/s00253-010-2544-0

Ghebreyesus, T. A., & Frieden, T. R. (2018). REPLACE: A roadmap to make the world *trans* fat free by 2023. *The Lancet, 391*(10134), 1978-1980. https://doi.org/10.1016/S0140-6736(18)31083-3

Green, R., & Rogers, E. J. (2013). Chapter twenty eight - Transformation of chemically competent *E. coli*. In J. Lorsch (Ed.), *Methods in enzymology* (pp. 329-336). Academic Press. https://doi.org/10.1016/B978-0-12-418687-3.00028-8

Guo, Q., Ha, Y., Li, Q., Jin, J., Deng, Z., Li, Y., & Zhang, S. (2015). Impact of additives on thermally-induced *trans* isomers in 9c,12c linoleic acid triacylglycerol. *Food Chemistry, 174*, 299-305. https://doi.org/10.1016/j.foodchem.2014.11.063

Heipieper, H., Diefenbach, R., & Keweloh, H. (1992). Conversion of *cis* unsaturated fatty acids to *trans*, a possible mechanism for the protection of phenol-degrading *Pseudomonas putida* P8 from substrate toxicity. *Applied and Environmental Microbiology, 58*(6), 1847-1852. https://doi.org/10.1128/aem.58.6.1847-1852.1992

Heipieper, H., Waard, P., Meer, P., Killian, J., Isken, S., Bont, J., . . . Wolf, F. (2001). Regiospecific

effect of 1-octanol on *cis-trans* isomerization of unsaturated fatty acids in the solvent-tolerant strain *Pseudomonas putida* S12. *Applied Microbiology and Biotechnology, 57*(4), 541-547. https://doi.org/10.1007/s002530100808

Hiranuma, N., Park, H., Baek, M., Anishchenko, I., Dauparas, J., & Baker, D. (2021). Improved protein structure refinement guided by deep learning based accuracy estimation. *Nature Communications, 12*(1), 1340. https://doi.org/10.1038/s41467-021-21511-x

Holtwick, R., Keweloh, H., & Meinhardt, F. (1999). *Cis*/*trans* isomerase of unsaturated fatty acids of *Pseudomonas putida* P8: Evidence for a heme protein of the cytochrome *c* type. *Applied and Environmental Microbiology, 65*(6), 2644-2649. https://doi.org/10.1128/aem.65.6.2644-2649.1999

Holtwick, R., Meinhardt, F., & Keweloh, H. (1997). *Cis-trans* isomerization of unsaturated fatty acids: Cloning and sequencing of the *cti* gene from *Pseudomonas putida* P8. *Applied and Environmental Microbiology, 63*(11), 4292-4297. https://doi.org/10.1128/aem.63.11.4292-4297.1997

Iida, H., Takahashi, K., Yanagisawa, A., Hashimoto, H., & Igarashi, A. (2021). Reduction of *trans* fatty acids in hydrogenated soybean oil using Ni/$TiO_2$ catalysts. *Food Chemistry, 340*, 127927. https://doi.org/10.1016/j.foodchem.2020.127927

Kan, S. B. J., Huang, X., Gumulya, Y., Chen, K., & Arnold, F. H. (2017). Genetically programmed chiral organoborane synthesis. *Nature, 552*(7683), 132-136. https://doi.org/10.1038/nature24996

Kim, B. H., & Akoh, C. C. (2015). Recent research trends on the enzymatic synthesis of structured lipids. *Journal of Food Science, 80*(8), C1713-C1724. https://doi.org/10.1111/1750-3841.12953

Kodali, D. R. (2014). 1 - *Trans* fats: Health, chemistry, functionality, and potential replacement solutions. In D. R. Kodali (Ed.), *Trans fats replacement solutions* (pp. 1-39). AOCS Press.

https://doi.org/10.1016/B978-0-9830791-5-6.50006-X

Kuhnt, K., Baehr, M., Rohrer, C., & Jahreis, G. (2011). *Trans* fatty acid isomers and the *trans*-9/*trans*-11 index in fat containing foods. *European Journal of Lipid Science and Technology, 113*(10), 1281-1292. https://doi.org/10.1002/ejlt.201100037

Mauger, M., Ferreri, C., Chatgilialoglu, C., & Seemann, M. (2021). The bacterial protective armor against stress: The *cis-trans* isomerase of unsaturated fatty acids, a cytochrome-*c* type enzyme. *Journal of Inorganic Biochemistry, 224*, 111564. https://doi.org/10.1016/j.jinorgbio.2021.111564

Mozaffarian, D., Aro, A., & Willett, W. C. (2009). Health effects of *trans*-fatty acids: Experimental and observational evidence. *European Journal of Clinical Nutrition, 63*(2), S5-S21. https://doi.org/10.1038/sj.ejcn.1602973

Mozaffarian, D., Katan, M. B., Ascherio, A., Stampfer, M. J., & Willett, W. C. (2006). *Trans* fatty acids and cardiovascular disease. *New England Journal of Medicine, 354*(15), 1601-1613. https://doi.org/10.1056/NEJMra054035

Muñoz-Rojas, J., Bernal, P., Duque, E., Godoy, P., Segura, A., & Ramos, J.-L. (2006). Involvement of cyclopropane fatty acids in the response of *Pseudomonas putida* KT2440 to freeze-drying. *Applied and Environmental Microbiology, 72*(1), 472-477. https://doi.org/10.1128/aem.72.1.472-477.2006

Nelson, K. E., Weinel, C., Paulsen, I. T., Dodson, R. J., Hilbert, H., Martins dos Santos, V. A. P., . . . Fraser, C. M. (2002). Complete genome sequence and comparative analysis of the metabolically versatile *Pseudomonas putida* KT2440. *Environmental Microbiology, 4*(12), 799-808. https://doi.org/10.1046/j.1462-2920.2002.00366.x

Okuyama, H., Ueno, A., Enari, D., Morita, N., & Kusano, T. (1997). Purification and characterization of 9-hexadecenoic acid *cis-trans* isomerase from *Pseudomonas* sp. strain E-3. *Archives of Microbiology, 169*(1), 29-35. https://doi.org/10.1007/s002030050537

Owji, H., Nezafat, N., Negahdaripour, M., Hajiebrahimi, A., & Ghasemi, Y. (2018). A comprehensive review of signal peptides: Structure, roles, and applications. *European Journal of Cell Biology, 97*(6), 422-441. https://doi.org/10.1016/j.ejcb.2018.06.003

Park, J.-Y., Choi, H.-W., Park, K.-M., & Chang, P.-S. (2023). An improved method for rapid evaluation of enzymatic *cis*/*trans* isomerization of $C_{18:1}$ monounsaturated fatty acids. *Food Chemistry, 404*, 134618. https://doi.org/10.1016/j.foodchem.2022.134618

Pedrotta, V., & Witholt, B. (1999). Isolation and characterization of the *cis-trans*-unsaturated fatty acid isomerase of *Pseudomonas oleovorans* GPo12. *Journal of Bacteriology, 181*(10), 3256-3261. https://doi.org/10.1128/jb.181.10.3256-3261.1999

Pettersen, E. F., Goddard, T. D., Huang, C. C., Couch, G. S., Greenblatt, D. M., Meng, E. C., & Ferrin, T. E. (2004). UCSF Chimera — A visualization system for exploratory research and analysis. *Journal of Computational Chemistry, 25*(13), 1605-1612. https://doi.org/10.1002/jcc.20084

Ramzi, A. B., Hyeon, J. E., & Han, S. O. (2015). Improved catalytic activities of a dye-decolorizing peroxidase (DyP) by overexpression of ALA and heme biosynthesis genes in *Escherichia coli*. *Process Biochemistry, 50*(8), 1272-1276. https://doi.org/10.1016/j.procbio.2015.05.004

Sharp, P. M., & Li, W.-H. (1987). The codon adaptation index - A measure of directional synonymous codon usage bias, and its potential applications. *Nucleic Acids Research, 15*(3), 1281-1295. https://doi.org/10.1093/nar/15.3.1281

Stevens, J. M., Mavridou, D. A. I., Hamer, R., Kritsiligkou, P., Goddard, A. D., & Ferguson, S. J. (2011). Cytochrome c biogenesis system I. *The FEBS Journal, 278*(22), 4170-4178. https://doi.org/10.1111/j.1742-4658.2011.08376.x

Tan, Z., Yoon, J. M., Nielsen, D. R., Shanks, J. V., & Jarboe, L. R. (2016). Membrane engineering via *trans* unsaturated fatty acids production improves *Escherichia coli* robustness and production of biorenewables. *Metabolic Engineering, 35*, 105-113. https://doi.org/10.1016/j.ymben.2016.02.004

Teufel, F., Almagro Armenteros, J. J., Johansen, A. R., Gíslason, M. H., Pihl, S. I., Tsirigos, K. D., . . . Nielsen, H. (2022). SignalP 6.0 predicts all five types of signal peptides using protein language models. *Nature Biotechnology, 40*(7), 1023-1025. https://doi.org/10.1038/s41587-021-01156-3

Thöny-Meyer, L. (1997). Biogenesis of respiratory cytochromes in bacteria. *Microbiology and Molecular Biology Reviews, 61*(3), 337-376. https://doi.org/10.1128/mmbr.61.3.337-376.1997

Thöny-Meyer, L., Fischer, F., Künzler, P., Ritz, D., & Hennecke, H. (1995). *Escherichia coli* genes required for cytochrome *c* maturation. *Journal of Bacteriology, 177*(15), 4321-4326. https://doi.org/10.1128/jb.177.15.4321-4326.1995

Tsuzuki, W., Matsuoka, A., & Ushida, K. (2010). Formation of *trans* fatty acids in edible oils during the frying and heating process. *Food Chemistry, 123*(4), 976-982. https://doi.org/10.1016/j.foodchem.2010.05.048

Varnado, C. L., & Goodwin, D. C. (2004). System for the expression of recombinant hemoproteins in *Escherichia coli*. *Protein Expression and Purification, 35*(1), 76-83. https://doi.org/10.1016/j.pep.2003.12.001

von Wallbrunn, A., Richnow, H. H., Neumann, G., Meinhardt, F., & Heipieper, H. J. (2003). Mechanism of *cis-trans* isomerization of unsaturated fatty acids in *Pseudomonas putida*. *Journal of Bacteriology, 185*(5), 1730-1733. https://doi.org/10.1128/jb.185.5.1730-1733.2003

Wilkes, R. S., & Bringe, N. A. (2015). Applications of trait enhanced soybean oils. In F. T. Orthoefer & G. R. List (Eds.), *Trait- modified oils in foods* (pp. 71-92). Wiley Blackwell. https://doi.org/10.1002/9781118961117.ch5

Wilks, J. C., & Slonczewski, J. L. (2007). pH of the cytoplasm and periplasm of *Escherichia coli*: Rapid measurement by green fluorescent protein fluorimetry. *Journal of Bacteriology, 189*(15), 5601-5607. https://doi.org/10.1128/jb.00615-07

Yamoneka, J., Malumba, P., Lognay, G., Blecker, C., & Danthine, S. (2019). Irvingia gabonensis seed

666 fat as hard stock to formulate blends for *trans* free margarines. *LWT, 101*, 747-756.
667 https://doi.org/10.1016/j.lwt.2018.11.053
668

**Figure captions**

**Fig. 1.** Overview of cloning strategy for *cis*/*trans* fatty acid isomerase (CTI) from *Pseudomonas putida* KT2440. (a) Primers used for overhang PCR amplification of CTI fragments from the genomic DNA (gDNA) of *P*. *putida* KT2440. (b) In-fusion cloning of CTI fragments with overhangs into pET26b(+) vectors linearized by two restriction enzymes (Nco1 and Xho1). (c) Genetic map of two plasmids used in this study. The CTI gene encoded in the constructed pET26b(+) plasmid can be expressed by IPTG induction, and CTI proteins are subsequently matured by the cytochrome *c* maturation system, which is constitutively expressed by pEC86 plasmid. (d) Schematic diagram for dual-transformation of the plasmids into *Escherichia coli* BL21(DE3) for heterologous expression of CTI proteins.

**Fig. 2.** Molecular cloning of the *cis*/*trans* fatty acid isomerase (CTI) gene from *Pseudomonas putida* KT2440. (a) Gradient PCR amplification of CTI fragments with overhangs. The DNA bands expected as amplified CTI genes (2,274 bp) were detected between 2.0 kb and 3.0 kb. The annealing temperature range was from 55.0$^{o}$C to 60.0$^{o}$C, and 60.0$^{o}$C was chosen (no detection of unspecific bands). M, DNA molecular marker. (b) In-fusion cloning of the CTI fragments into pET26b(+) plasmids. Lane 1, linearized pET26b(+) plasmid (5,360 bp, Xho1); Lane 2, linearized pET26b(+) plasmid with the CTI fragments (7,538 bp, Xho1); Lane 3, linearized pET26b(+) plasmid with the CTI fragments (7,538 bp, Nde1, Xho1). (c) Dual-transformation of pET26b(+) plasmid with the CTI fragments (7,538 bp) and pEC86 (11,753 bp) plasmid into *Escherichia coli* BL21(DE3). Lane 1, plasmids purified from *E*. *coli* BL21(DE3) dual-transformants and linearized by restriction enzymes (Nco1, Xho1).

**Fig. 3.** Heterologous expression and purification of *cis*/*trans* fatty acid isomerase (CTI) from *Pseudomonas putida* KT2440. (a) Predicted structural features of the putative CTI recombinant protein. The

original N-terminal signal peptide of CTI was replaced with the pelB signal peptide, and the polyhistidine tag ($His_6$) for purification was attached to the C-terminus. (b) Computational prediction of signal peptide and cleavage site (CS, dash dot line) of the putative CTI recombinant protein. The subregion probability of n-region (circle), h-region (square), c-region (diamond), and non-signal peptide region (triangle) at each amino acid position was predicted. Sec/SP1, the secretory signal peptides transported by the Sec translocon and cleaved by signal peptidase I. (c, d) Purification of his-tagged CTI proteins by a FPLC equipped with an Ni-NTA affinity column. Cleared lysates extracted from transformants were resolved with a linear imidazole gradient (10–500 mM). (e) SDS-PAGE analysis of eluted proteins in each fraction. The protein bands expected as CTI recombinant proteins (approximately 86 kDa) were detected between 75 kDa and 100 kDa. M, protein molecular marker; Lane 1, total cell proteins; Lane 2, insoluble proteins; Lane 3, cleared lysate; Lane 4, unbound fraction (integrated 3–12 fractions, 1.0 mL/fraction); Lane 5–16, imidazole-eluted fractions (26–37 fractions, 0.5 mL/fraction); Lane 17, purified his-tagged CTI proteins (integrated 28–30 pure fractions) after dialysis and concentration.

**Fig. 4.** Control of the *cis*/*trans* isomerism of unsaturated fatty acids by the *cis*/*trans* fatty acid isomerase (CTI) recombinant protein. (a) Time-course of the production of *trans*-monounsaturated fatty acids from each *cis*-monounsaturated fatty acid (substrate) until reaction equilibration. EA, elaidic acid ($C_{18:1}$, *trans*-$\Delta^9$); VA, vaccenic acid ($C_{18:1}$, *trans*-$\Delta^{11}$); PEA, palmitelaidic acid ($C_{16:1}$, *trans*-$\Delta^9$). (b) Conversion rate (%) of *cis* configuration to *trans* configuration after the CTI reaction. Asterisk denotes significant differences between the data ($p<0.05$, Duncan's multiple range test). OA, oleic acid ($C_{18:1}$, *cis*-$\Delta^9$); cVA, *cis*-vaccenic acid ($C_{18:1}$, *cis*-$\Delta^{11}$); POA, palmitoleic acid ($C_{16:1}$, *cis*-$\Delta^9$).

**Fig. 5.** Optimum reaction conditions for the *cis*/*trans* fatty acid isomerase (CTI) recombinant protein against palmitoleic acid ($C_{16:1}$, *cis*-$\Delta^9$). (a) Effects of reaction pH (2.0−11.0) on the reaction. Different

buffers were used to control each range of reaction pH condition. Sodium acetate (circle, pH 2.0−6.0); Potassium phosphate (square, pH 6.0−8.0); Tris-HCl (diamond, pH 8.0−9.0); Glycine-NaOH (triangle, pH 9.0−11.0). (b) Effects of reaction temperature (5−60℃) on the reaction. All reactions were conducted at the optimal pH condition. Asterisk denotes significant differences between the data ($p<0.05$, Duncan's multiple range test).

**Fig. 6.** Enzyme kinetic analysis of the *cis*/*trans* isomerization of palmitoleic acid ($C_{16:1}$, *cis*-$\Delta^9$) by the *cis*/*trans* fatty acid isomerase (CTI) recombinant protein. (a) Michaelis-Menten plot of the CTI reaction. The initial velocity ($v$) at each substrate concentration (0.10–1.20 mM) was derived from a linear regression of the time-course data of the CTI reaction (0–30 min). (b) Hanes-Woolf double-reciprocal plot of the reaction. All reactions were conducted at the optimal reaction pH and temperature.

**Fig. 7.** Predicted three-dimensional structure model of the *cis*/*trans* fatty acid isomerase (CTI) recombinant protein and its proposed catalytic mechanism. Two cysteine residues of the heme-binding motif (CVACH, 46–50 amino acid residues) in the putative cytochrome *c* domain (33–190 amino acid residues, brick red) can be covalently linked to heme by two thioether bonds after cytochrome *c* maturation. (For interpretation of the color, the reader should be referred to the web version of this paper.)

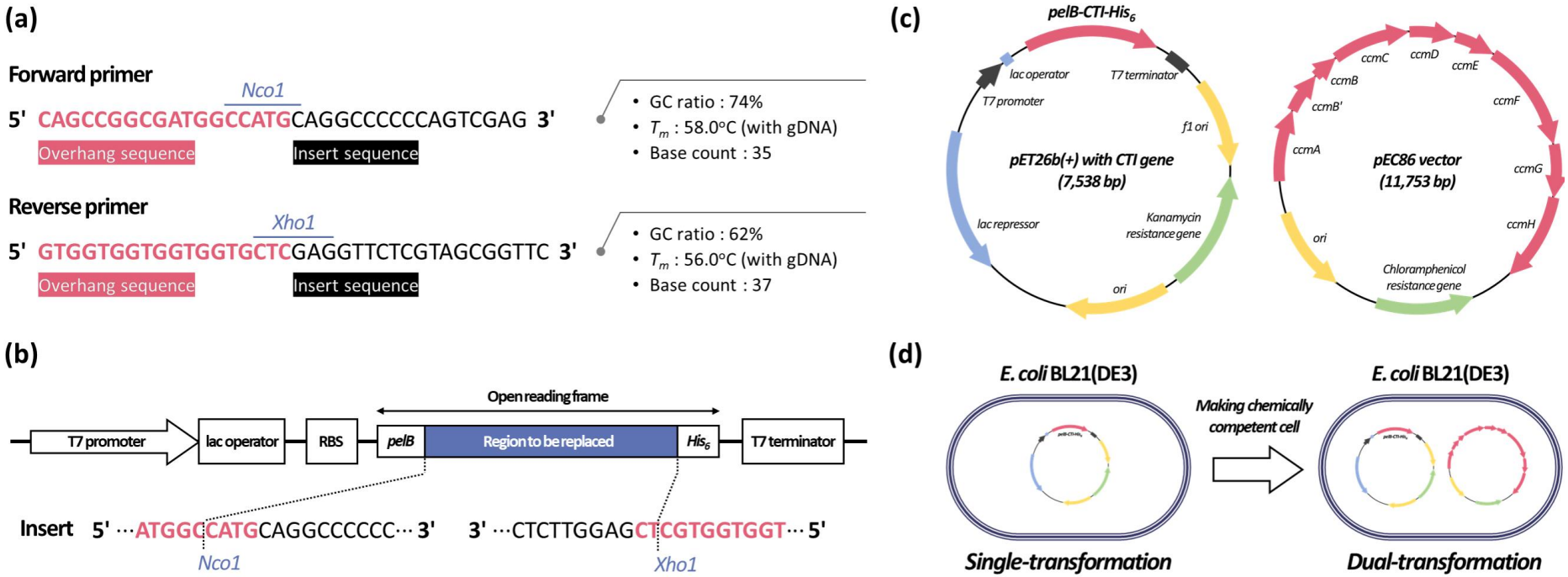
(a)
Forward primer
Nco1
5' CAGCCGGCGATGGCCATGCAGGCCCCCCAGTCGAG 3'
Overhang sequence
Insert sequence
• GC ratio : 74%
• $T_m$ : 58.0°C (with gDNA)
• Base count : 35
Reverse primer
Xho1
5' GTGGTGGTGGTGGTGCTCGAGGTTCTCGTAGCGGTTC 3'
Overhang sequence
Insert sequence
• GC ratio : 62%
• $T_m$ : 56.0°C (with gDNA)
• Base count : 37
(b)
Open reading frame
T7 promoter
lac operator
RBS
pelB
Region to be replaced
His6
T7 terminator
Insert 5' ···ATGGCCATGCAGGCCCCCC··· 3'
3' ···CTCTTGGAGCTCCGTGGTGGT··· 5'
Nco1
Xho1
(c)
pelB-CTI-His6
lac operator
T7 terminator
T7 promoter
f1 ori
pET26b(+) with CTI gene
(7,538 bp)
lac repressor
Kanamycin
resistance gene
ori
ccmC
ccmD
ccmE
ccmB
ccmB'
ccmF
ccmA
pEC86 vector
(11,753 bp)
ccmG
ccmH
ori
Chloramphenicol
resistance gene
(d)
E. coli BL21(DE3)
Making chemically
competent cell
E. coli BL21(DE3)
Single-transformation
Dual-transformation

Fig. 1.

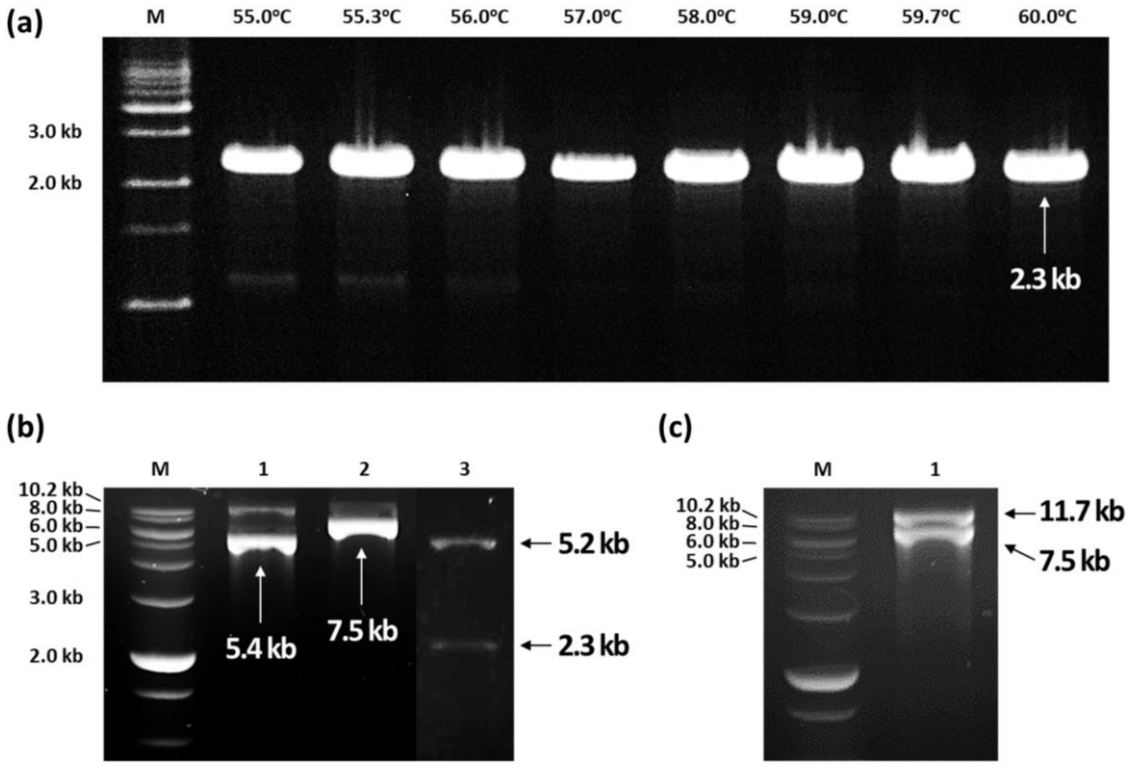
(a)
M
55.0°C
55.3°C
56.0°C
57.0°C
58.0°C
59.0°C
59.7°C
60.0°C
3.0 kb
2.0 kb
2.3 kb
(b)
M
1
2
3
10.2 kb
8.0 kb
6.0 kb
5.0 kb
3.0 kb
2.0 kb
5.4 kb
7.5 kb
5.2 kb
2.3 kb
(c)
M
1
10.2 kb
8.0 kb
6.0 kb
5.0 kb
11.7 kb
7.5 kb

Fig. 2.

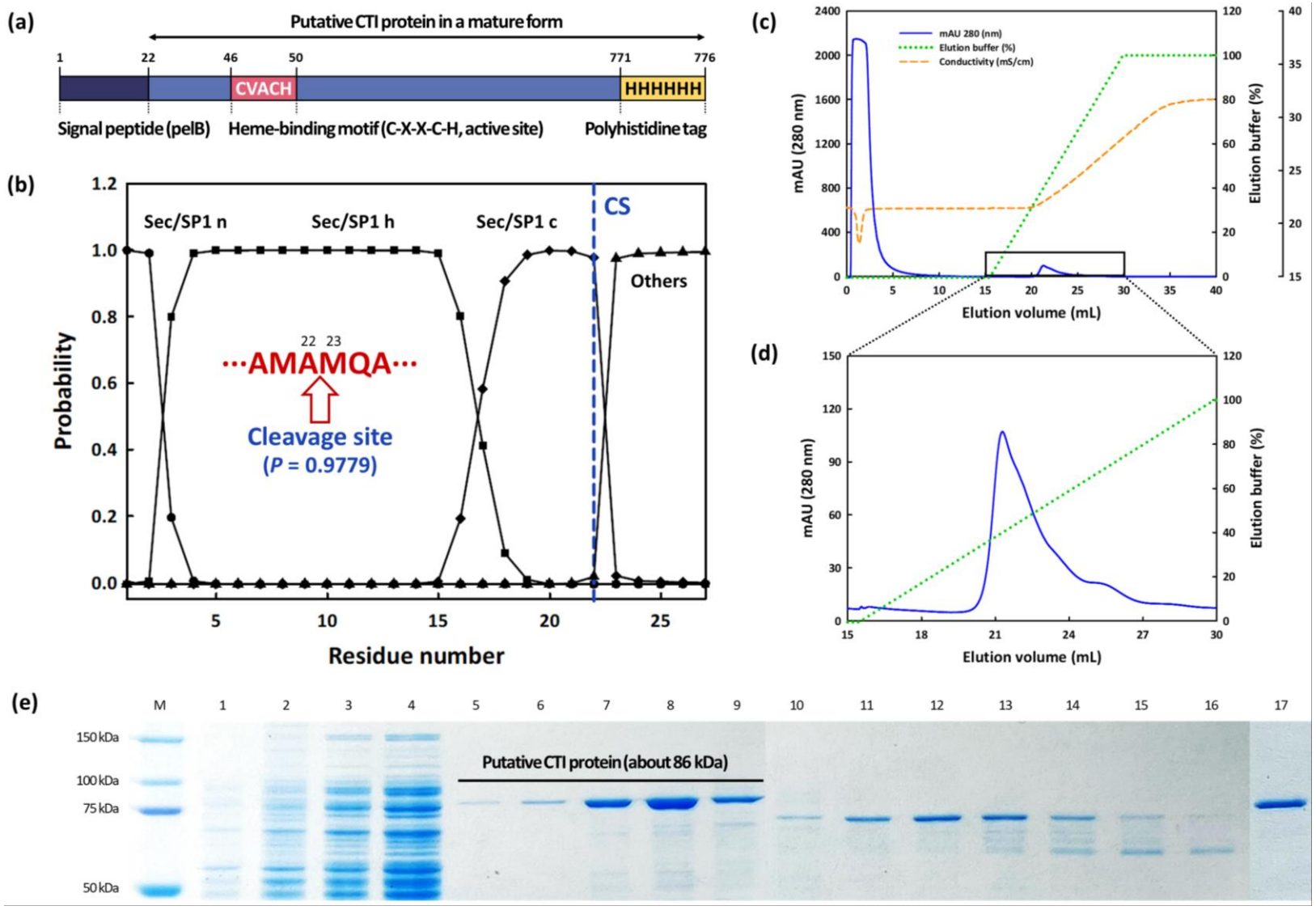
(a)
Putative CTI protein in a mature form
1
22
46
50
771
776
CVACH
HHHHHH
Signal peptide (pelB)
Heme-binding motif (C-X-X-C-H, active site)
Polyhistidine tag
(b)
Sec/SP1 n
Sec/SP1 h
Sec/SP1 c
CS
Others
22 23
···AMAMQA···
Cleavage site
(P = 0.9779)
Probability
Residue number
(c)
mAU 280 (nm)
Elution buffer (%)
Conductivity (mS/cm)
mAU (280 nm)
Elution buffer (%)
Elution volume (mL)
(d)
mAU (280 nm)
Elution buffer (%)
Elution volume (mL)
(e)
M
1
2
3
4
5
6
7
8
9
10
11
12
13
14
15
16
17
150 kDa
100 kDa
75 kDa
50 kDa
Putative CTI protein (about 86 kDa)

Fig. 3.

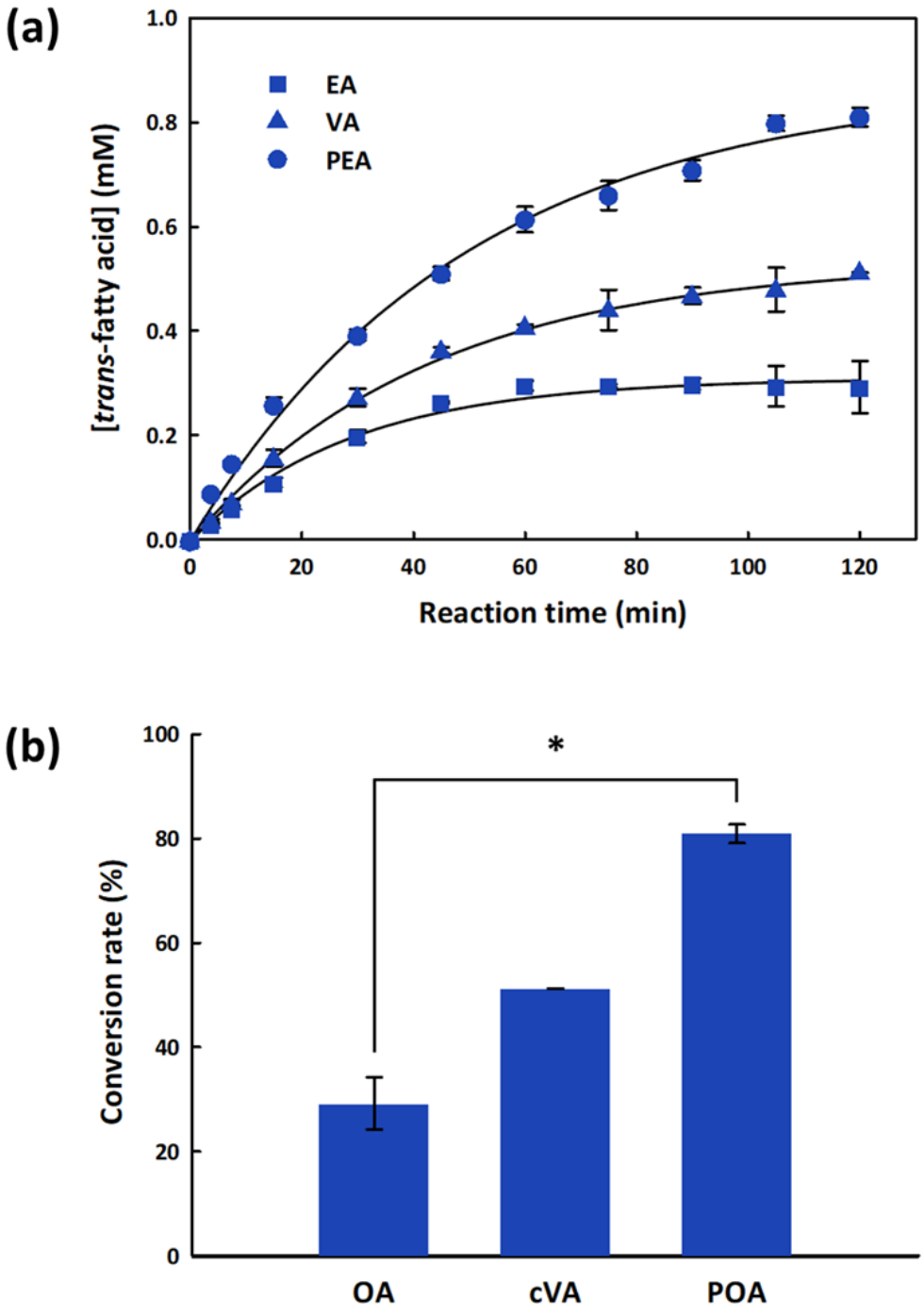
(a)
1.0
0.8
0.6
0.4
0.2
0.0
[trans-fatty acid] (mM)
EA
VA
PEA
0
20
40
60
80
100
120
Reaction time (min)
(b)
100
80
60
40
20
0
Conversion rate (%)
*
OA
cVA
POA

Fig. 4.

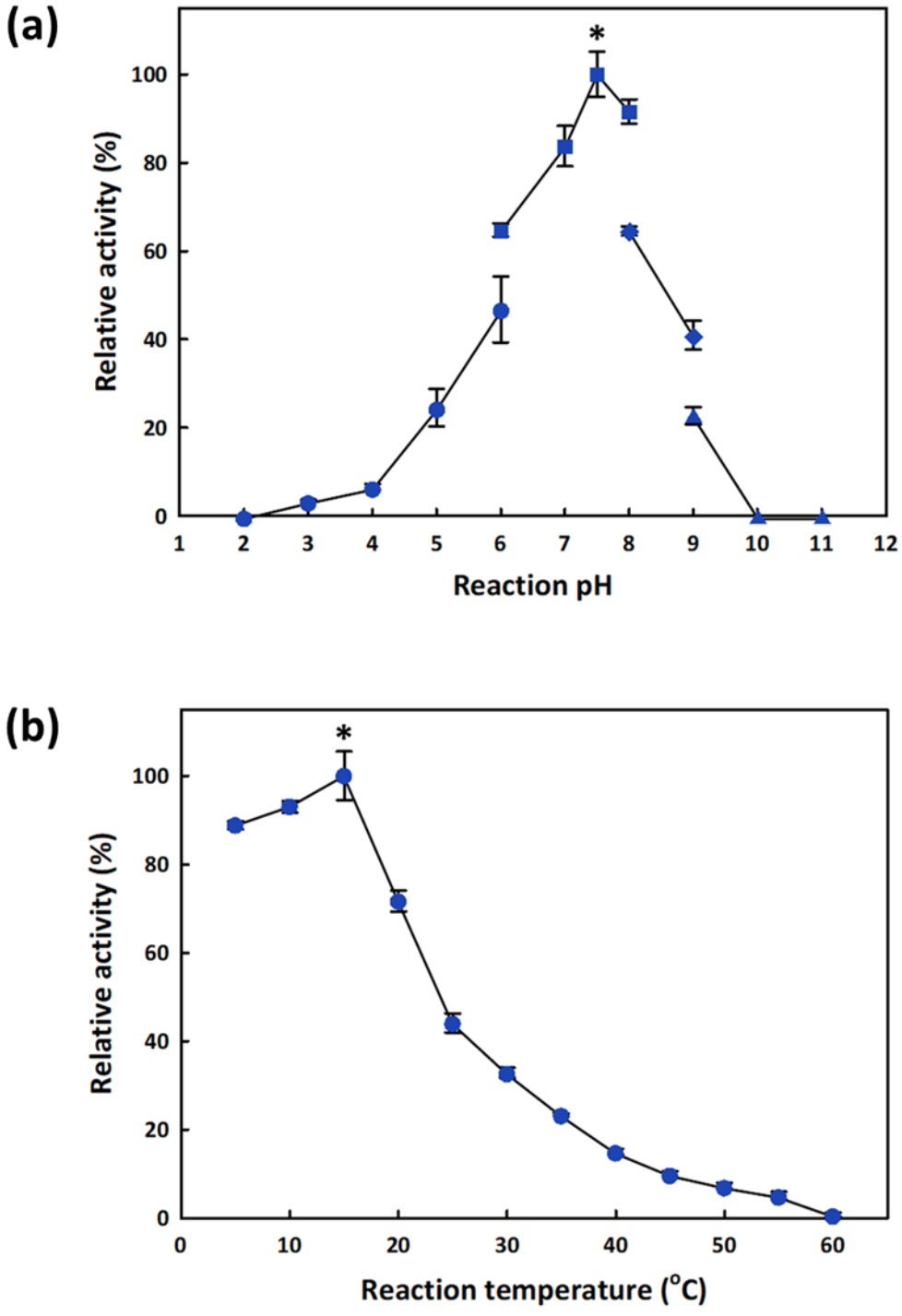
(a)
Relative activity (%)
Reaction pH
(b)
Relative activity (%)
Reaction temperature (°C)

Fig. 5

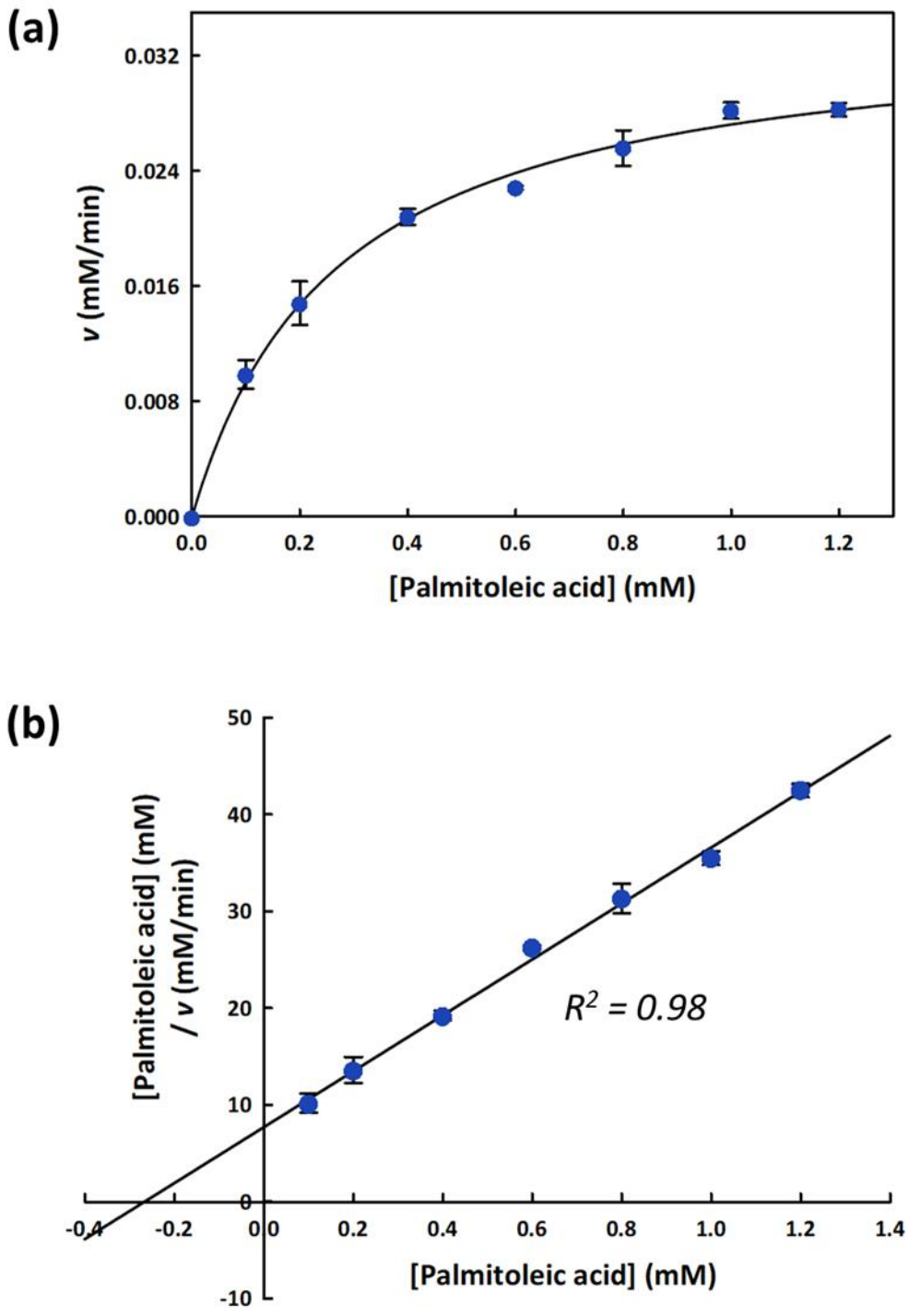
(a)
0.032
0.024
0.016
0.008
0.000
v (mM/min)
0.0
0.2
0.4
0.6
0.8
1.0
1.2
[Palmitoleic acid] (mM)
(b)
50
40
30
20
10
0
-10
[Palmitoleic acid] (mM) / v (mM/min)
R2 = 0.98
-0.4
-0.2
0.0
0.2
0.4
0.6
0.8
1.0
1.2
1.4
[Palmitoleic acid] (mM)

Fig. 6

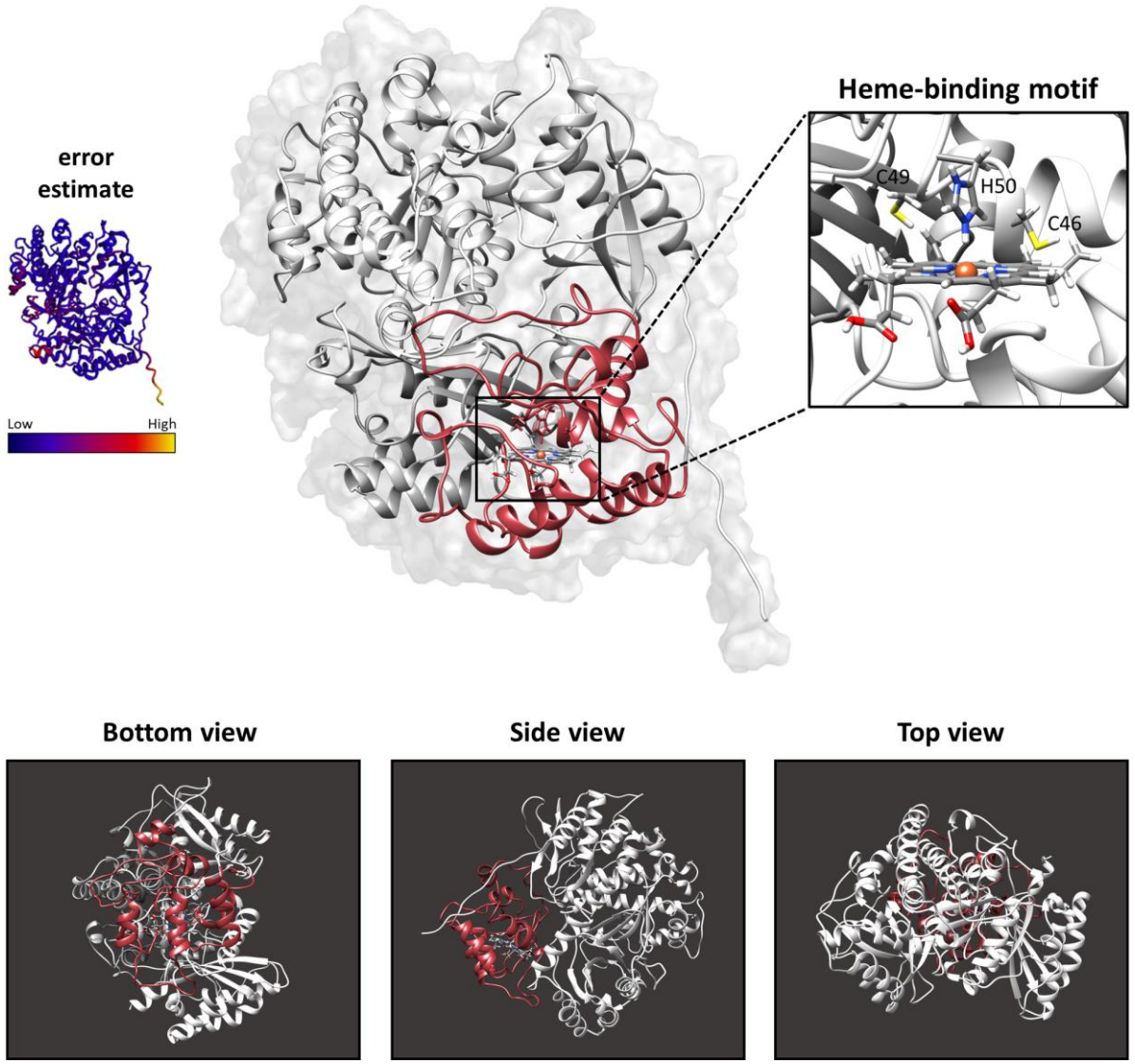
error
estimate
Low
High
Heme-binding motif
C49
H50
C46
Bottom view
Side view
Top view

Fig. 7.

## Highlights

- *Cis*/*trans* fatty acid isomerase (CTI) is a bacterial cytochrome *c*-type hemoprotein.
- The recombinant CTI was expressed in the pET26b/pEC86 co-expression system.
- The recombinant CTI showed substrate promiscuity towards unsaturated fatty acids.
- The recombinant CTI showed strong substrate selectivity against palmitoleic acid.
- Deep learning-based structural prediction demonstrated the mode of action of CTI.

**Declaration of Interests**

☒ The authors declare that they have no known competing financial interests or personal relationships that could have appeared to influence the work reported in this paper.

☐The authors declare the following financial interests/personal relationships which may be considered as potential competing interests:

**CRediT Authorship Contribution Statement**

**Jun-Young Park**: Conceptualization, Investigation, Data curation, Writing - Original draft, Writing - Review & Editing, Visualization. **Yun-Seo Jung**: Investigation, Validation, Formal analysis, Writing - Review & Editing. **Dimitris Charalampopoulos**: Writing - Review & Editing. **Kyung-Min Park**: Writing - Review & Editing, Project administration, Funding acquisition. **Pahn-Shick Chang**: Conceptualization, Writing - Review & Editing, Supervision, Project administration.

# Controlling *cis*/*trans* isomerism of monounsaturated fatty acids via a recombinant cytochrome *c*-type *cis*/*trans* fatty acid isomerase

Jun-Young Park[1], Yun-Seo Jung[1], Dimitris Charalampopoulos,

Kyung-Min Park[*], Pahn-Shick Chang[*]

This document file contains Supplementary Data (S1−S8).

**Supplementary Data Table S1.** The detailed operating condition for the gas chromatography-flame ionization detector (GC-FID) analysis

| Parameters | Conditions |
|---|---|
| GC equipment | YL6500GC system |
| Column | DB-FastFAME |
| Length/internal diameter | 30 m/0.25 mm |
| Film thickness | 0.25 μm |
| Carrier gas | Helium |
| Mode | 1.0 mL/min (constant flow mode) |
| Inlet | |
| Temperature | 250℃ |
| Split ratio | 50:1 |
| FID | |
| Temperature | 250℃ |
| Gas profile | Hydrogen: 40 mL/min |
| | Zero-air: 300 mL/min |
| | Make-up gas (nitrogen): 25 mL/min |
| Injection volume | 1 μL |
| Oven temperature | 80℃(1.0 min)→40℃/min to 200℃(6.0 min) |
| Total run time | 10 min |

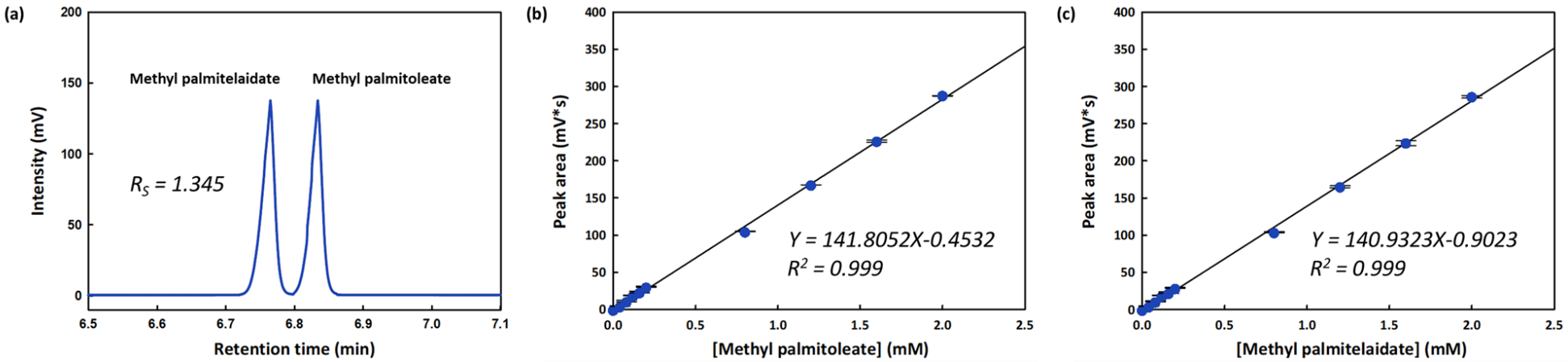


**Supplementary Data Fig. S2.** Chromatographic resolution of palmitoleic acid and palmitelaidic acid using a GC-FID equipped with a cyanopropyl phase DB-FastFAME capillary column. (a) The GC-FID chromatogram of the mixture of methyl palmitoleate and methyl palmitelaidate dissolved in *n*-hexane at the same molar concentration (1 mM). (b) Calibration curve of methyl palmitoleate. (c) Calibration curve of methyl palmitelaidate.

ATGAAATACCTGCTGCCGACCGCTGCTGCTGGTCTGCTGCTCCTCGCTGCCCAGCCGGCGATGGCCATGCAGGCCCCCCAGTCGAGCCCG

GCTATTTCCTACACCCGGGACATTCAACCGATCTTCACCGAGAAGTGCGTGGCCTGCCACGCCTGCAACGACGCCGCCTGCCAGCTCAAG

CTGGAAAGCCCTGAAGGCGCGGTACGCGGGGCCAGCAAGGTCCCGGTGTACCAGGGCGAGCGGAGCAAGGCAGTCCCCACCACGCGGC

TGTTCTACGACGCACACAGCGAAGAGCAATGGCGCAAGAAGGGCTTCTACTCGGTGCTCGACAACCAGGGCGGTCAGGCCGCGTTGATG

GCGCGCATGCTGGAGTTGGGCCACAAGACCCCGCTTACGCCCAACGCCAAGCTGCCCGAAGAGATCGTCCTGGGCCTGAGCCGCAACAA

CATGTGCCCGTTGCCCCATGAATTCGACGCCTATGCCGGCGCACACCCCAAGGAGGGCATGCCGCTGGCGGTGACCGGGCTGACCGACAA

GGAATATGACACCATGCGCCGCTGGCTGGCCGCTGGTGCGCCGGTGGAGTACCAGCCGATCCAGCCGAGCGCGGCCGAAGCCAGGCAGA

TCGCAGAGTGGGAAGAACTGCTCAACCGCCCGGGTTCCACCGAGGCGCTGGTGGGACGCTGGCTGTACGAGCACCTGTTTTTGGCGCAC

ATCCATTTCGCTGGCGGCGAGCAGGGCCACTTCTTCCAGTGGGTGCGCTCGCGCACGCCAAGTGGCAAGCCGGTCGATATCATTGCCACC

CGCCGCCCCAACGACCCACCGGGCACGGACTTCTACTACCGGTTGATCCCGGTGCAGGGCGTGATCGTGCACAAGACGCACATCACCTAC

CCGATGGGGCCGCAGAAGCTCAAGCGCGTGAAGCAGCTGTTCTATGCCGGTGACTGGCATGCTGCCGCGCTTCCGGGCTACGGCCCGCG

CCACCGGGCCAATCCGTTTGAAACCTTCGAGGCGATCCCGGCGGTGGCGCGCTACCAGTTCATGCTGGATAACGCCGAGTACTTCGTGCG

CACCTTCATCCGTGGCCCGGTGTGCCGCGGGCAGATTGCCACCGACGTGATCCGCGACAACTTCTGGGCGCTGTTCCAGGAGCCGGCCTT

CGATCGCTACATCACCGATGCCAAGTACCGCGGCGAGGCTACCCCGCTGCTGGCCATGCCTGGTCAGATCGATGACGTGGGCAGTGTGCT

GAGCCTGTGGCACGCCTATCGTGACAAGCGCAACGACTACGAGAAACTGCGCCGTGAAGCCTATGCCGAAATGCCGGCACCGAGATGGT

CGACGCTGTGGGCCGGTAACGACAATGCGCTGCTGAGCATCTTCCGTCACTTCGACAGCGCATCGGTGACCAAGGGCCTGGTGGGGGAT

GTGCCGCTGACCGTGTGGCTGTTCGACTACCCGTTGTTCGAGCGCACGTATTACCAGCTGGCGGTCAACTTCGATGTGTATGGCAACGTTT
CGCACCAGTTGCAGACGCGCCTGTATTTCGACCTGATCCGCAACGGCGCCGAGGTCAACTTCCTGCGCCTGATGCCGGCCGACCAGCGCA
AGGCGATCCTTGGCGACTGGTACCAGAACAGTGGCAAGGTGAAGATGTGGATGGATTATGAAGACATCGACACCGACACCCCGAGTGGC
ATCAAGCTCGACCCGCGCAACCCCAAACGCGACTTTGGACTGAAGCTGCTGCAGCGCACCGGCAGCCTGAATGCCGCACCGGACCCGAT
CAACCGCTGCCAGGGCGCGTTCTGCTCACGGCCGCAGATGAGCGAAGAATTCCGCAATGCCGAGCAGTCGCTCAGCCGACTGGTGTCAC
GCCCGGCGGCCGGGCTGAAGGTGATCAACCAGTTGCCCGAGGCGACCATGCTGCGTATCGAAGGGCAGGACGGCCAGCGTCAGGTGTAC
AGCCTGCTGCGCAACCGCGCGCACAGCAACGTGGCGTTCCTGCTGGGTGAGGCGTACCGCTACCAGCCGGGGCTGGATACCCTGACCCT
GTACCCGGGGGTGCTCTCCAGCTACCCGAACTTCATCTTCAACATCCCGACCAAGGATGTGCCGGAGTTCGTCGAGGACATGGAGTACGC
CAAAGATGACGCGGCGAAGTTCGAGCGCATTGTCATGCGCTGGGGTGTGCGCCGCAGTCACCCGGCCTTCTGGCGCTATTTCCATGACCT
GAACAGCTATATCAAGGAGACCGAACCGGTCGAGGCGGGCGTGCTGGACATGAACCGCTACGAGAACCTCGAGCACCACCACCACCACC
ACTGA

**Supplementary Data Fig. S3.** Nucleotide sequence of an open reading frame for the *cis*/*trans* fatty acid isomerase recombinant gene in the constructed pET26b(+) plasmid.

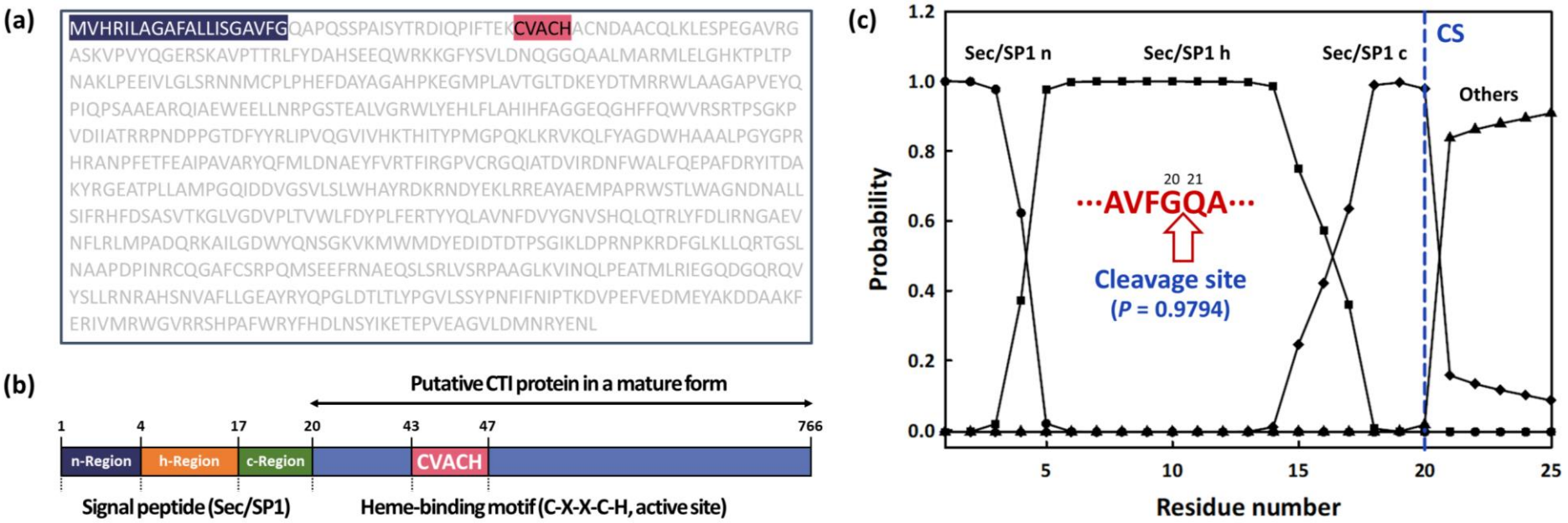


**Supplementary Data Fig. S4.** Genome-based structural analysis of wildtype *cis*/*trans* fatty acid isomerase (CTI) from *Pseudomonas putida* KT2440. (a) Full amino acid sequence of CTI from *P. putida* KT2440. (b) Predicted structural features of CTI. This protein is a putative cytochrome *c*-type protein (87 kDa) with an iron-containing heme binding motif (CVACH, red) and a Sec/SP1 signal peptide (1−20 residues). Sec/SP1, the secretory signal peptides transported by the Sec translocon and cleaved by signal peptidase I. (c) Computational prediction of signal peptide and cleavage site (CS, dash dot line) of CTI. The subregion probability of n-region (circle), h-region (square), c-region (diamond), and non-signal peptide region (triangle) was predicted.

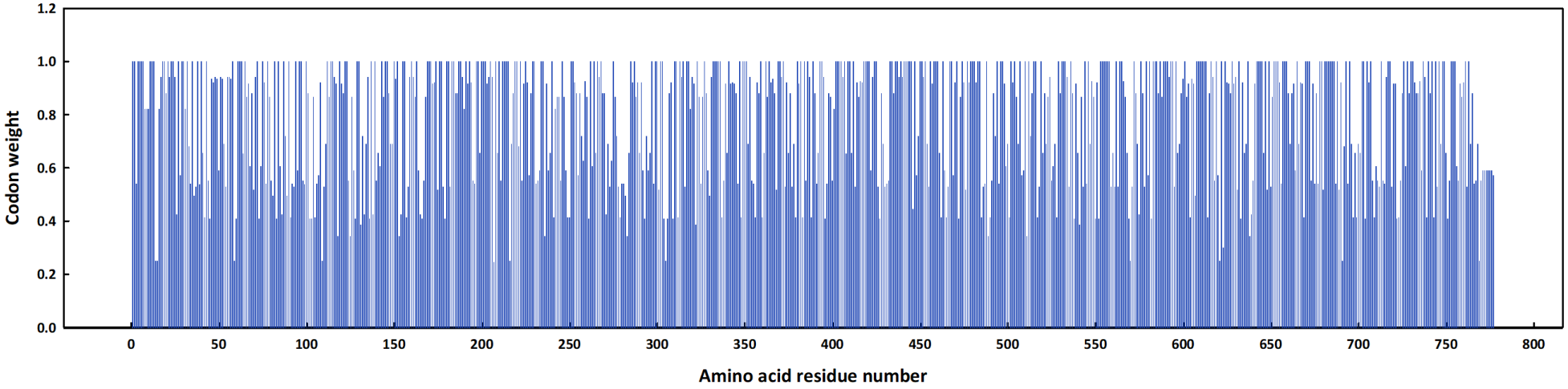


**Supplementary Data Fig. S5.** Codon weights of each amino acid residue of the *cis*/*trans* fatty acid isomerase gene cloned in *Escherichia coli* BL21(DE3).

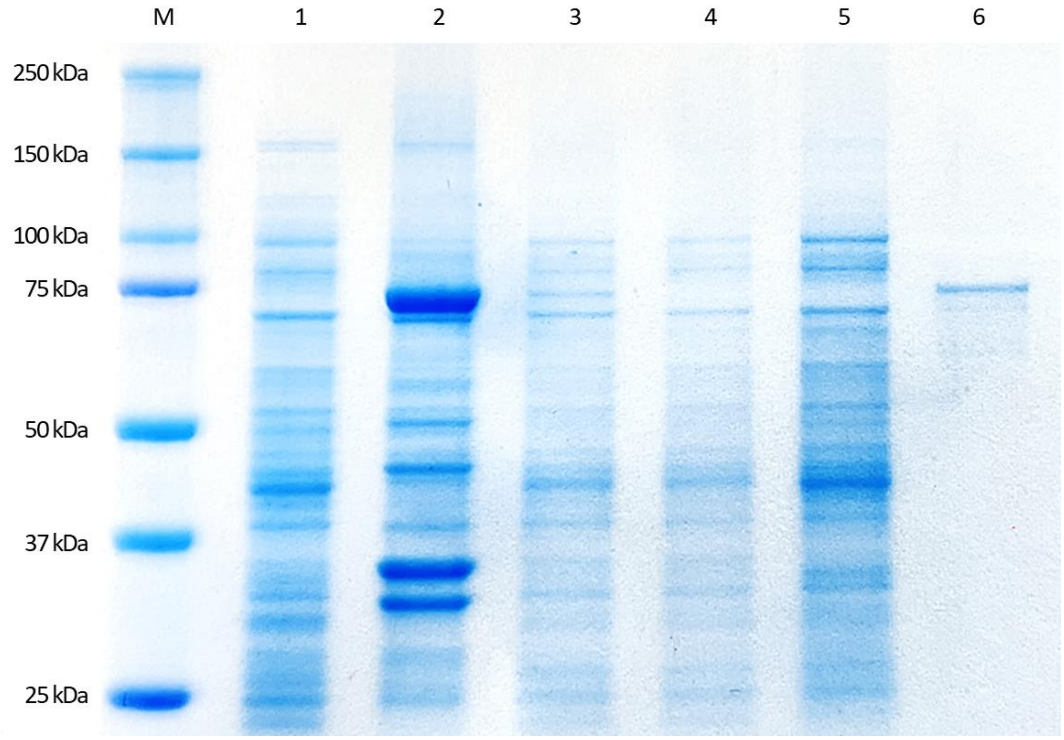


**Supplementary Data Fig. S6.** Heterologous expression and purification of *cis*/*trans* fatty acid isomerase from *Pseudomonas putida* KT2440 in the pET26b expression system. The protein bands expected as the recombinant proteins were detected below 75 kDa. M, protein molecular marker; Lane 1, soluble fraction; Lane 2, insoluble fraction; Lane 3, solubilized fraction using a cationic 1%(w/v) CHAPS detergent; Lane 4, unbound fraction (20 mM imidazole); Lane 5, washed fraction (40 mM imidazole); Lane 6, eluted fraction (250 mM imidazole).

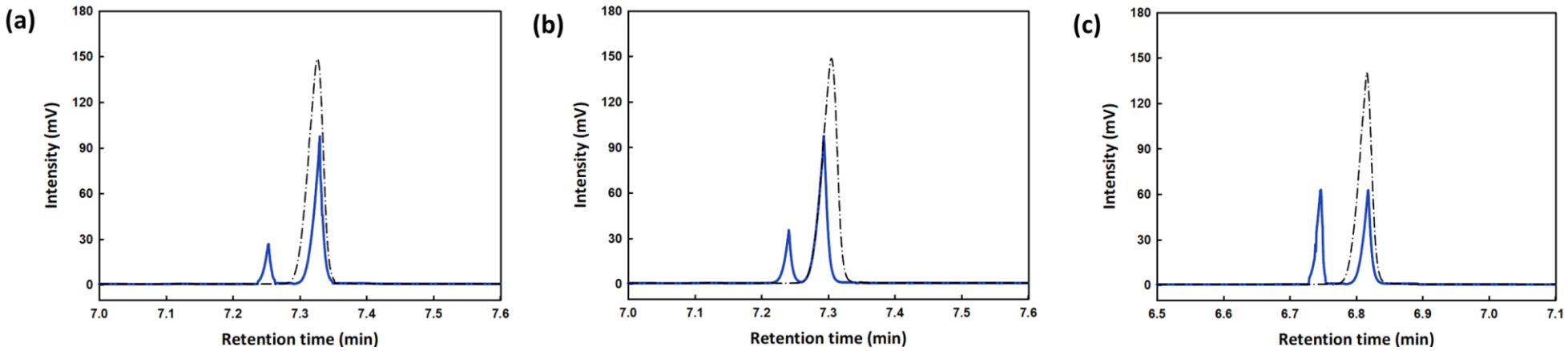


**Supplementary Data Fig. S7.** GC-FID analysis of the reactants from the *cis*/*trans* isomerization of three monounsaturated fatty acids by *cis*/*trans* fatty acid isomerase recombinant protein. (a) The GC-FID chromatogram of the methylated fatty acids before (dash dot line) and after (straight line) the 30 min reaction with 1 mM oleic acid ($C_{18:1}$, *cis*-$\Delta^9$). (b) The GC-FID chromatogram of the methylated fatty acids before (dash dot line) and after (straight line) the 30 min reaction with 1 mM *cis*-vaccenic acid ($C_{18:1}$, *cis*-$\Delta^{11}$). (c) The GC-FID chromatogram of the methylated fatty acids before (dash dot line) and after (straight line) the 30 min reaction with 1 mM palmitoleic acid ($C_{16:1}$, *cis*-$\Delta^9$).

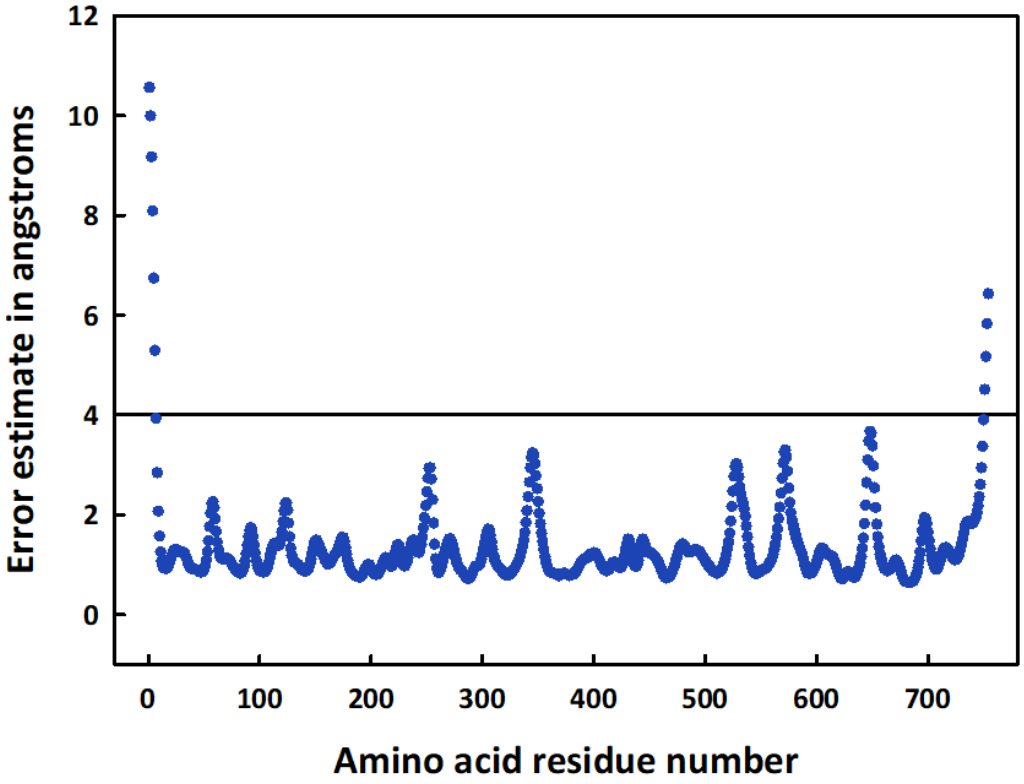


**Supplementary Data Fig. S8.** Angstrom error per amino acid residue in the predicted structure of the *cis*/*trans* fatty acid isomerase recombinant protein. The predicted structure is considered to be highly confident.

## Graphical Abstract